



HAL
open science

The Effect of Normal Stress Oscillations on Fault Slip Behavior Near the Stability Transition From Stable to Unstable Motion

Federico Pignalberi, Carolina Giorgetti, Corentin Noël, Chris Marone,
Cristiano Collettini, Marco Maria Scuderi

► **To cite this version:**

Federico Pignalberi, Carolina Giorgetti, Corentin Noël, Chris Marone, Cristiano Collettini, et al.. The Effect of Normal Stress Oscillations on Fault Slip Behavior Near the Stability Transition From Stable to Unstable Motion. *Journal of Geophysical Research: Solid Earth*, 2024, 129 (2), 10.1029/2023JB027470 . hal-04456699

HAL Id: hal-04456699

<https://hal.science/hal-04456699v1>

Submitted on 15 Feb 2024

HAL is a multi-disciplinary open access archive for the deposit and dissemination of scientific research documents, whether they are published or not. The documents may come from teaching and research institutions in France or abroad, or from public or private research centers.

L'archive ouverte pluridisciplinaire **HAL**, est destinée au dépôt et à la diffusion de documents scientifiques de niveau recherche, publiés ou non, émanant des établissements d'enseignement et de recherche français ou étrangers, des laboratoires publics ou privés.



Distributed under a Creative Commons Attribution 4.0 International License

JGR Solid Earth

RESEARCH ARTICLE

10.1029/2023JB027470

Key Points:

- Normal stress perturbations modulate fault strength and slip behavior
- High frequency, high amplitude oscillations generate dynamic weakening
- Rate and state friction laws predict the laboratory results

Supporting Information:

Supporting Information may be found in the online version of this article.

Correspondence to:

F. Pignalberi,
federico.pignalberi@uniroma1.it

Citation:

Pignalberi, F., Giorgetti, C., Noël, C., Marone, C., Collettini, C., & Scuderi, M. M. (2024). The effect of normal stress oscillations on fault slip behavior near the stability transition from stable to unstable motion. *Journal of Geophysical Research: Solid Earth*, 129, e2023JB027470. <https://doi.org/10.1029/2023JB027470>

Received 15 JULY 2023
Accepted 26 JAN 2024

Author Contributions:

Conceptualization: Federico Pignalberi, Cristiano Collettini, Marco Maria Scuderi
Data curation: Federico Pignalberi, Marco Maria Scuderi
Formal analysis: Federico Pignalberi, Carolina Giorgetti, Corentin Noël
Funding acquisition: Chris Marone, Marco Maria Scuderi
Investigation: Federico Pignalberi, Marco Maria Scuderi
Methodology: Federico Pignalberi, Marco Maria Scuderi
Supervision: Chris Marone, Marco Maria Scuderi
Visualization: Federico Pignalberi, Carolina Giorgetti, Corentin Noël, Marco Maria Scuderi
Writing – original draft: Federico Pignalberi

© 2024. The Authors.

This is an open access article under the terms of the [Creative Commons Attribution License](https://creativecommons.org/licenses/by/4.0/), which permits use, distribution and reproduction in any medium, provided the original work is properly cited.

The Effect of Normal Stress Oscillations on Fault Slip Behavior Near the Stability Transition From Stable to Unstable Motion

Federico Pignalberi¹ , Carolina Giorgetti¹ , Corentin Noël^{1,2} , Chris Marone^{1,3} , Cristiano Collettini^{1,4} , and Marco Maria Scuderi¹ 

¹Dipartimento di Scienze della Terra, La Sapienza Università di Roma, Rome, Italy, ²Observatoire de la Côte d'Azur, IRD, Géoazur, CNRS, Université de Côte d'Azur, Valbonne, France, ³Department of Geosciences, Pennsylvania State University, University Park, PA, USA, ⁴Istituto Nazionale di Geofisica e Vulcanologia (INGV), Rome, Italy

Abstract Tectonic fault zones are subject to normal stress variations with a wide range of spatio-temporal scales. Stress perturbations cover a wide range of frequencies and amplitudes from high frequency seismic waves generated by earthquakes to low frequency transients associated with solid Earth tides. These perturbations can reactivate critically stressed faults and trigger earthquakes. Here, we describe lab experiments to illuminate the physics of such changes in friction and the mechanics of earthquake triggering and fault reactivation. Friction tests were done in a double direct shear configuration for conditions near the stability transition from stable to unstable motion. We studied simulated fault gouge composed of quartz powder and conducted experiments at reference normal stress from 10 to 13.5 MPa. After shearing to steady state sliding, we applied sinusoidal normal stress oscillations of amplitude 0.5–2 MPa, and period of 0.5–50 s. We performed numerical simulations using measured values of rate and state friction (RSF) parameters to assess our data. Our results show that low frequency stress oscillations cause a Coulomb-like response of shear strength that transitions from stable slip to slow lab earthquakes as frequency increases. At the critical frequency predicted by RSF we observe periodic stick-slip behavior. Perturbations of high amplitude and short period weaken the fault, while lower amplitudes strengthen the fault. We find that a modified RSF formulation is able to accurately match our laboratory data. Our findings highlight the complex effects of stress perturbations on fault strength and the mode of fault slip.

Plain Language Summary Tectonic fault zones are subjected to transient stress perturbations that propagate in the Earth's crust. These stress changes have the potential to reactivate fault zones and can occur at different frequencies and amplitudes, ranging from seismic waves generated by earthquakes to smaller perturbations associated with Earth tides. To investigate this phenomenon, we conducted laboratory experiments using quartz powder to simulate a fault zone. During the experiment, we subjected the fault to sinusoidal stress oscillations with various amplitudes (0.5–2 MPa) and periods (0.5–50 s). Our results show that faults, under critical conditions, exhibit a variety of slip behaviors depending on the oscillation amplitude and frequency. We found that stress perturbations with high amplitude and short period are able to weaken the fault and generate fast instabilities, while lower amplitudes strengthen the fault. To accurately explain our laboratory findings, we developed a rate and state friction formulation, which successfully matched our experimental results. In conclusion, our study sheds light on the complex effects of stress perturbations on fault strength and the mode of fault slip. By understanding these dynamics, we enhance our understanding of earthquake triggering and fault reactivation, which has important implications for earthquake hazard assessment.

1. Introduction

The recurrence time of earthquakes together with tectonic loading can be influenced by small stress variations arising from external perturbations such as: slip on a nearby fault (e.g., Stein et al., 1992), seismic wave passing through a rock volume (e.g., Gombert et al., 1997, 1998), geo-reservoir exploitation (e.g., Ellsworth, 2013), seasonal hydrology (e.g., Bettinelli et al., 2008), Earth tides (e.g., Scholz et al., 2019), etc. These perturbations can vary in space and time to produce the critical stress conditions for earthquake triggering (Freed, 2005). Stress perturbations can vary over a wide range of amplitudes and frequencies, spanning from the high frequencies of seismic waves to the low frequencies of tides. Thus, the causal relation between stress perturbation and earthquake triggering or fault slip is often obscure. To relate frictional rheology to stress perturbation, previous work,

Writing – review & editing:

Federico Pignalberi, Carolina Giorgetti,
Corentin Noël, Chris Marone,
Cristiano Colletini, Marco Maria Scuderi

based on the coupling of experimental and theoretical approaches, has revealed important factors, including the critical period of stress perturbations, that may control fault stability (Beeler & Lockner, 2003; Boettcher & Marone, 2004; Hong & Marone, 2005; Rice & Ruina, 1983; Richardson & Marone, 1999). However, there is still not a comprehensive set of observations that can generate a consistent physical framework to explain earthquake stress triggering.

Earth Tides, with their low amplitude and frequency have proven difficult to relate to earthquake triggering and occurrence. A correlation with Earth tides has been found mainly in the shallow crust (Cochran et al., 2004; Scholz et al., 2019) but generally under special conditions. Deeper in the crust, it has been demonstrated that the amplitude of the stress variations induced by tides is not sufficient to impact seismicity rate (Beeler & Lockner, 2003; Scholz, 2003; Vidale et al., 1998), and the correlation with earthquakes is not high enough for statistical validation (e.g., Rydelek et al., 1992). However, other works have demonstrated that quasi-dynamic modes of fault slip, such as slow-slip and tremor, appear to be more sensitive to small stress variations (Hawthorne & Rubin, 2010; Lambert et al., 2009; Nakata et al., 2008; Rubinstein et al., 2008; Thomas et al., 2009). In some cases, these modes of fault slip can be used as stress meters (J. Dieterich et al., 2000) in a manner similar to that suggested for changes in earthquake frequency-magnitude relations (e.g., Gulia & Wiemer, 2019). Previous works show that tremor can arise from small perturbation of shear stress generated by Earth tides (Lambert et al., 2009; Thomas et al., 2009). Other works show that sometimes tremor rate increases with the passage of seismic waves (Miyazawa & Brodsky, 2008; Miyazawa & Mori, 2005; Peng et al., 2009; Rubinstein et al., 2007) and in general that the seismicity rate can increase due to the passage of seismic waves from distant earthquakes, for example, after: 1992 Landers M_w 7.3 (Gomberg et al., 1997; Hill et al., 1993); 1999 M_w 7.4 Izmit (Ellsworth & Bulut, 2018); 2002 M_w 7.9 Denali (Gomberg et al., 2004); 2012 M_w 8.6 east Indian Ocean (Pollitz et al., 2012).

The effect of external stress perturbations on friction and fault slip behavior, including dynamic triggering, has been studied in the laboratory using a variety of protocols: stepwise variations in normal stress (J. H. Dieterich & Linker, 1992; Hong & Marone, 2005; Kilgore et al., 2017; Linker & Dieterich, 1992; Shreedharan et al., 2019); shear stress oscillations (Lockner & Beeler, 1999; Savage and Marone, 2007, 2008); normal stress oscillations (Boettcher & Marone, 2004; Richardson & Marone, 1999); pore fluid oscillations (Chanard et al., 2019; Noël, Passelègue, et al., 2019; Noël, Pimienta, & Violay, 2019); or acoustic vibration (Johnson et al., 2008). These studies show that triggering is a function of the amplitude and frequency of the stress perturbation. Here, we expand these works to a wider range of boundary conditions and study in particular the fault response to stress oscillations near the stability transition between stable and unstable frictional sliding. We focus on three questions: (a) How do normal stress oscillations change the slip behavior of a critically stressed fault? (b) Can normal stress perturbations reduce fault friction and act as a trigger to unstable slip? (c) Can RSF predict the laboratory results under a broad range of complex conditions?

2. Fault Stability Theory and Stress Perturbations

Rate and state friction (RSF) laws provide a description of fault sliding behavior during perturbations in slip rate, normal stress, and state (J. H. Dieterich, 1979, 1981; Linker & Dieterich, 1992; Marone, 1998; Rice, 1983; Ruina, 1983):

$$\mu(\theta, \sigma_n, V) = \mu_0 + a \ln\left(\frac{V}{V_0}\right) + b \ln\left(\frac{V_0 \theta}{D_c}\right) \quad (1)$$

where, μ_0 represents the steady state friction at a reference shear velocity V_0 , and a and b are dimensionless constants that scale the change in friction with velocity at constant state, θ , and the evolution of friction over a characteristic slip distance D_c , respectively. The state parameter θ accounts for friction memory effects related to the history of slip. To describe the frictional response to changes in sliding velocity V or normal stress (σ_n), Equation 1 must be coupled with a state evolution law:

$$\frac{d\theta}{dt} = 1 - \frac{V\theta}{D_c} - \frac{a\theta}{b\sigma_n} \frac{d\sigma_n}{dt} \quad (\text{Dieterich or Aging law}) \quad (2)$$

$$\frac{d\theta}{dt} = -\frac{V\theta}{D_c} \ln\left(\frac{V\theta}{D_c}\right) - \frac{\alpha\theta}{\sigma_n b} \frac{d\sigma_n}{dt} \quad (\text{Ruina or Slip Law}) \quad (3)$$

The friction law (Equation 1) and evolution law (Equation 2 or 3) must be coupled with a relation that describes the elastic interaction between the sliding surface and the elastic surrounding. Neglecting inertia, the one-dimensional single degree of freedom elastic interaction is described by the relation (Tullis & Weeks, 1986):

$$\frac{d\mu}{dt} = k'(V_{lp} - V_f) \quad (4)$$

where k' is the fault loading stiffness normalized by normal stress, V_{lp} is the load point velocity, and V_f is the fault slip velocity. Following the RSF framework, fault stability is controlled by the ratio of a critical weakening rate with slip $(b - a)/D_c$ and the loading stiffness k' . If $(b - a) < 0$ the system responds to an increase in velocity with an increase in friction (i.e., velocity strengthening) and the system is intrinsically stable. However, if $(b - a) > 0$ friction decreases with increasing shear velocity (i.e., velocity weakening), and the fault stability depends on a critical fault weakening rate sometimes referred to as a critical rheologic stiffness, k_c :

$$k_c = \frac{(b - a) \sigma_n}{D_c} \quad (5)$$

The parameter k_c represents the rate of fault weakening with slip. The stability of sliding therefore depends on the ratio of k/k_c (e.g., Gu et al., 1984; Leeman et al., 2016; Rice & Ruina, 1983).

In the context of RSF, the stability of frictional sliding exhibits a bifurcation when the elastic stiffness of the surrounding k (equivalent to the host rock and fault zone stiffness) is less than the critical fault weakening rate k_c (equivalent to the fault stiffness) (Gu et al., 1984; Rice & Ruina, 1983). Therefore, the stiffness ratio $\kappa = k/k_c$ defines the transition from stable, when $\kappa > 1$, to unstable motion, when $\kappa < 1$. If $\kappa < 1$ the stored elastic energy will be released dynamically and the slip will be unstable. On the other hand, if $\kappa > 1$ the elastic unloading is greater than the critical stiffness and stable, aseismic motion is predicted. At the bifurcation, when $\kappa \sim 1$, complex fault slip behaviors are predicted (Baumberger et al., 1994; Gu & Wong, 1994; Gu et al., 1984; Heslot et al., 1994), and these include slow slip events and period doubling as documented in laboratory experiments (Leeman et al., 2016, 2018; Mele Veedu et al., 2020; Scuderi et al., 2016).

To account for changes in normal stress during fault motion, Linker and Dieterich (1992) developed an approach to relate normal stress perturbations and frictional state. This approach has been studied extensively in the laboratory to evaluate the evolution of state (θ) (Boettcher & Marone, 2004; Hong & Marone, 2005; Kilgore et al., 2012, 2017; Linker & Dieterich, 1992; Richardson & Marone, 1999; Shreedharan et al., 2019). Linker and Dieterich (1992) described the evolution of frictional state with time (t) following a variation in normal stress (σ_n) via the term α that quantifies the magnitude of the shear stress response to a step change in normal stress, given by:

$$\alpha = \frac{\Delta\tau_\alpha}{\sigma_n^f} \frac{1}{\ln\left(\frac{\sigma_n^f}{\sigma_n^0}\right)} \quad (6)$$

$$\theta = \theta_0 \left(\frac{\sigma_{\text{initial}}}{\sigma_{\text{final}}}\right)^{\frac{\alpha}{b}} \quad (7)$$

where σ_n^0 is the initial value of normal stress, σ_n^f is the normal stress after the step and $\Delta\tau_\alpha$ is the transient variation in shear stress following the normal stress step (Hong & Marone, 2005; Shreedharan et al., 2019). We note that Equations 2 and 3, which contain time derivatives of the normal stress, cannot be used directly for step changes in normal stress, where the derivative is undefined, and thus Equations 6 and 7 are used along with the standard state evolution equation without the term containing α . The parameter α describes the inelastic evolution of state (with time or shear displacement) upon a step change in normal stress (Linker & Dieterich, 1992; Richardson & Marone, 1999) and it depends on fault mineralogy and other factors (e.g., Hong & Marone, 2005).

The parameter α can vary from 0 to the steady state friction (μ_{ss}) (Perfettini et al., 2001). A value close to zero gives an immediate response and maximum amplitude of the shear stress, while values close to the steady state friction (μ_{ss}) imply minimal shear stress response. Laboratory measurements of α range from 0.2 to 0.3 (Hong & Marone, 2005; Linker & Dieterich, 1992; Richardson & Marone, 1999; Shreedharan et al., 2019).

Perfettini et al. (2001) used theoretical and numerical approaches to study the effect of normal stress oscillations on the frictional stability of a creeping fault. They found that a fault under critically stable conditions (i.e., $k/k_c \sim 1$) can be destabilized by a resonance phenomenon when the frequency and amplitude of the normal stress perturbation reach some critical values. In this context, the critical period T_c (analogue in time of D_c) needed to destabilize slip is defined as:

$$T_c = \left(\frac{D_c}{V}\right) 2\pi \sqrt{\frac{a}{(b-a)}} \quad (8)$$

Note that, for $T < T_c$ the shear zone is in continuous evolution, leading to a constant evolution of θ . The critical amplitude, ε_c , representing the minimum amplitude of the perturbation required to destabilize the system, is defined as Perfettini et al. (2001):

$$\varepsilon_c = \frac{(b-a)}{\mu_{ss}} \frac{1 - \frac{k}{k_c}}{\sqrt{1 + \left(1 - \frac{\alpha}{\mu_{ss}}\right)^2 \frac{(b-a)}{a}}} \quad (9)$$

Therefore, under $k/k_c \sim 1$ and $\varepsilon > \varepsilon_c$ conditions, the slip behavior depends on the perturbation period. In this context, one expects that long period oscillations ($T > T_c$) will produce a Coulomb-like shear stress response in which frictional strength responds proportionally to normal stress changes and this is confirmed by experiment (Boettcher & Marone, 2004). Whereas for short period oscillations ($T < T_c$) friction does not change because the normal stress change is shorter than the time (or slip) required for frictional state evolution. Instead, at the critical period ($T = T_c$) fault destabilization can emerge with complex stick-slip motion (Boettcher & Marone, 2004; Perfettini et al., 2001). However, there are relatively few lab studies that document frictional behavior during stress perturbations near the stability transition. In particular, the difficulty of achieving reproducible laboratory conditions where $k/k_c \sim 1$ has only been solved recently (Leeman et al., 2016; Scuderi et al., 2016; Shreedharan et al., 2020). Here we significantly expand the range of stress perturbations and conditions near $k/k_c \sim 1$ to understand the mechanics and compare laboratory results with theory.

To test frictional theory and gain insights on the mechanics underpinning stress triggering, we performed laboratory experiments on a simulated fault gouge composed of quartz powder. Under the starting condition of $k/k_c \sim 1$, we test a wide range of normal stress oscillation amplitudes and frequencies, comparing the laboratory results with the theoretical background described above in an attempt to link observations and theory.

3. Methods

3.1. Experimental Method

We performed laboratory experiments using a biaxial apparatus, BRAVA (Collettini et al., 2014), under room temperature and controlled 100% humidity conditions, in a double direct-shear configuration (Figure 1). All experiments (Table 1) are performed using quartz powder (Min-U-Sil 40, U.S. Silica Co.) composed of 99.5% SiO₂ and trace amounts of metal oxides, having a medium grain size of 10.5 μm . This material has been widely used in previous works and its mechanical and microstructural behavior is well documented (e.g., Bedford & Faulkner, 2021; Scuderi et al., 2016, 2017). In particular, it has been shown that Min-U-Sil has a transition from velocity strengthening to weakening during the early stages of deformation (i.e., shear strain $\gamma < 5$). Previous works document the critical fault rheologic stiffness (k_c) and thus we modulate the effective loading stiffness k to match this value and produce loading conditions where $k/k_c \sim 1$.

In our experiments, two 3-mm thick gouge layers are sandwiched between three steel forcing blocks characterized by two stationary side blocks (friction area $50 \times 50 \text{ mm}^2$) and a central forcing block ($80 \times 50 \text{ mm}^2$ size, see inset in Figure 1). The forcing blocks contain grooves perpendicular to the shear direction (0.8 mm high and 2 mm spacing) to ensure shear localization within the gouge layers and not at the boundary with the steel blocks. The

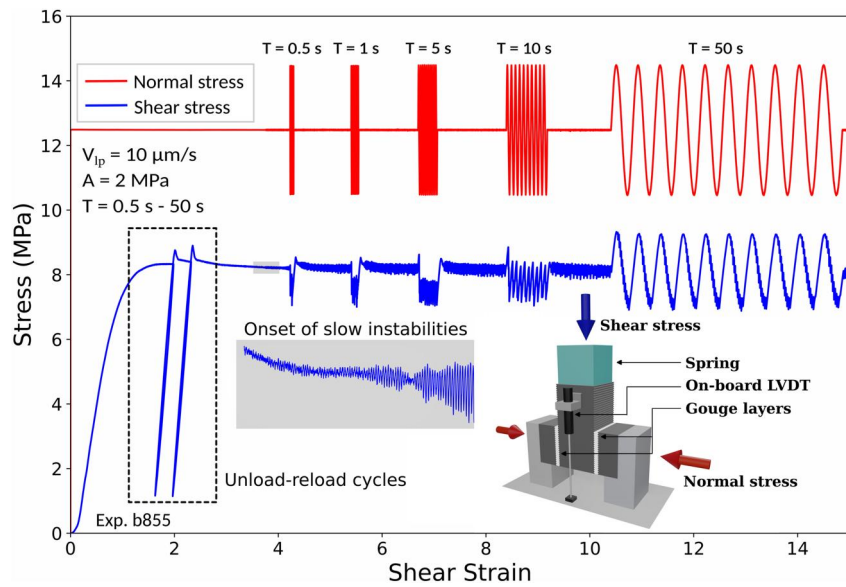


Figure 1. Data for one complete experiment (b855) showing shear stress (blue) and normal stress (red) as function of fault shear strain. Insert shows the double direct shear configuration. The dashed black rectangle (lower left) shows unloading-loading cycles performed to hasten achievement of steady state frictional sliding. Note normal stress oscillations of 2 MPa amplitude and a range of periods from 0.5 to 50 s.

biaxial apparatus consists of two orthogonal servo-controlled load frames with hydraulic pistons to apply load. The horizontal axis provides fault normal stress and the vertical axis provides fault shear stress (see inset Figure 1). Each piston is equipped with a strain gauge load cell (LEANE International model CCDG-0.1-100-SPEC) to measure the applied forces with an accuracy of 0.03 kN and a maximum force of 1.5 MN. Displacement transducers (Linear Variable Differential Transformer, LVDT) are fixed between the load frame and the moving piston and are used to measure the movement of the piston with an accuracy of 0.01 μm . An additional LVDT, with an accuracy of $\pm 0.01 \mu\text{m}$, was mounted directly on the sample assembly in the vertical direction to measure fault slip close to the simulated fault gouge (inset in Figure 1). The load point displacement measurements are corrected for the elastic deformation of the experimental apparatus (i.e., 386.12 kN/mm for the vertical frame and 329.5 kN/mm for the horizontal frame). All the output signals of load and displacement are recorded using a simultaneous multi-channel analog-to-digital converter with 24-bit/channel resolution at a maximum recording rate of 10 kHz. To decrease the shear loading stiffness of the apparatus and match the condition $k/k_c \sim 1$, we used an acrylic block in series between the vertical ram and the central forcing block (e.g., Scuderi et al., 2016 and see inset in Figure 1). The acrylic block we used has a stiffness of $6.35 \times 10^{-2} \text{ kN}/\mu\text{m}$ and shows a linear elastic deformation from 13 kN (equivalent to a shear stress of 2.6 MPa) up to 62.5 kN (equivalent to a shear stress of 12.5 MPa).

Table 1
Summary of the Experimental Conditions and Parameters

Exp. name	σ_n^{mean} (MPa)	A (MPa)	T (s)	μ_{ss}
b851	13.5	0.5	1–5–10–50	0.644
b852	12.5	0.5–1	0.5–1–5–10–50	0.660
b853	12.5	1	0.5–1–5–10–50–100	0.657
b854	12.5	1	0.5–1–5–10–50	0.660
b855	12.5	2	0.5–1–5–10–50	0.657
b856	10	2	0.5–1–5–10–50	0.669
b864	8	0.5–1	0.5–1–5–10–50	0.630

Note. σ_n^{mean} is the mean value of normal stress at which the oscillations are performed, A is the oscillation amplitude, T is the oscillation period and μ_{ss} is the value of steady state friction.

3.2. Experimental Procedure

Each experiment followed a common, computer controlled, deformation history (Figure 1). First, the normal stress was applied by advancing the horizontal ram in displacement feedback control until a small force was applied to the sample (usually 1 kN). Then, the feedback to the piston was switched from displacement to load control, to maintain a constant force, and the normal stress was increased stepwise to the target values of 8, 10, 12.5, or 13.5 MPa (Table 1).

These values of normal stresses were chosen because Scuderi et al. (2016) showed that, for the same gouge material and experimental conditions, they correspond to the boundary for frictional stability, where $k/k_c \sim 1$. Shear deformation was induced by advancing the vertical piston at a controlled displacement rate of 10 $\mu\text{m}/\text{s}$ to apply shear stress to the fault.

During the early stages of loading, the shear stress increased linearly with shear displacement (Figure 1). We normalize shear displacement by layer thickness and report shear strain $\gamma = \Sigma dx/h$, where dx is an increment of fault shear displacement and h is the instantaneous layer thickness. When the friction reached ~ 0.6 , sample yielding was marked by a deviation from the linear behavior, which usually took place after ~ 3 mm of displacement, followed by a short strain weakening evolution to a steady state frictional sliding. Values of frictional steady state are usually in the range $\mu_{ss} = 0.65 \pm 0.02$, consistent with previous studies (Leeman et al., 2016; Scuderi et al., 2016, 2017). Before starting the normal stress oscillations, we performed two cycles of unloading/loading to measure the fault stiffness and promote the formation of a steady state shear fabric. The fault stiffness is taken as the mean slope of the linear portions of the two unloading/loading cycles during the loading phase, and it was found to be $k = 0.0127$ MPa/ μm .

Scuderi et al. (2016) show consistently that the fault gouge evolves from velocity strengthening to velocity weakening in the early stages of deformation until reaching a steady velocity weakening for shear strain $\gamma \sim 6$. Matching the critical fault rheologic stiffness, k_c , with a spring to decrease apparatus stiffness, k , they found that the transition from stable sliding to slow-slip events takes place at a normal stress of 14 MPa, which corresponds to $k/k_c \sim 1$. Using the frictional parameters from Scuderi et al. (2016) after a shear strain of 14 we derive the critical rheological stiffness $k_c = 0.092$ MPa/ μm . Following this approach, our experiments were performed on velocity weakening material, at a stiffness ratio close to 1 ($\kappa = 1.38$), which corresponds to the transition between conditionally stable and unstable sliding.

3.3. Normal Stress Perturbation

After a shear strain of 4, steady state frictional sliding was well established and we began to see the spontaneous onset of small slow slips events (note onset of slow instabilities in Figure 1). At this point, we performed a series of sinusoidal normal stress oscillations around the mean value of normal stress (Table 1). Our normal stress oscillations always began with increasing normal stress. We tested the effect of oscillation amplitude, varying from 0.5 MPa, 1–2 MPa, and the period, varying from 0.5, 1, 5, 10, 50, and 100 s (Table 1). Each normal stress oscillation test lasted for at least 10 cycles and was separated from the previous by at least 2 mm of shear displacement to ensure steady state shearing prior to and after the test. This allowed us to evaluate each set of normal stress oscillations independently, without influence from the stress history. For each amplitude, the period was increased from short to long (Figure 1 and Table 1). Additionally, we tested the effect of strain accumulation by performing the reverse sequence with long period oscillations first.

4. Results

4.1. Parametrization of the Shear Stress Response

To quantify the frictional response to normal stress perturbations, for each set of oscillations, we use three parameters (Figure 2) (Boettcher & Marone, 2004): (a) The variation in frictional strength, $\Delta\tau$, during each cycle of normal stress oscillations; (b) The variation in peak yield strength, $\Delta\tau_{\text{yield}}$ corresponding to the difference between the peak (i.e., yield strength) in shear stress during the oscillations and the steady state shear stress at constant normal stress (measured as the average of the shear stress values between oscillation series); (c) The phase lag, $\Delta\phi$, corresponding to the time difference between the peak in shear stress and the peak in normal stress during the oscillations.

To compare between different experiments performed at different mean normal stress and remove small sample variability, $\Delta\tau$ and $\Delta\tau_{\text{yield}}$ are normalized by the oscillation semi-amplitude (0-to-peak) (A) and the steady state friction (μ_{ss}), while $\Delta\phi$ is converted to degrees:

$$\Delta\tau' = \frac{\Delta\tau}{2A\mu_{ss}} \quad (10)$$

$$\Delta\tau_{\text{yield}}' = \frac{\Delta\tau_{\text{yield}}}{A\mu_{ss}} \quad (11)$$

$$\Delta\phi = \frac{t_{\tau}^{\text{max}} - t_{\sigma_n}^{\text{max}}}{T} * 360 \quad (12)$$

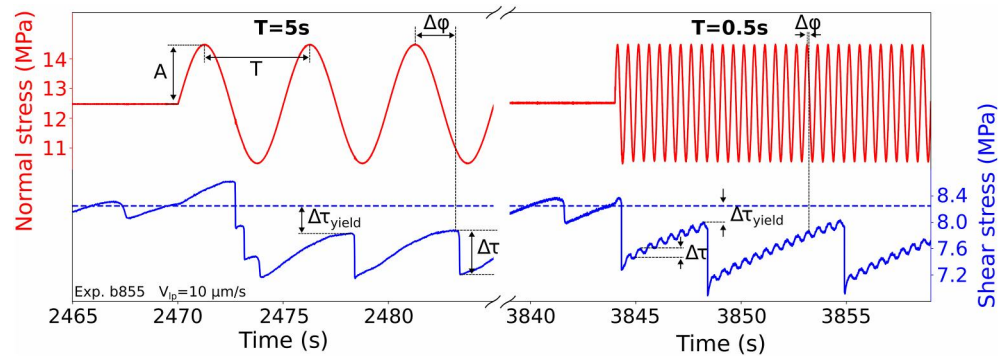


Figure 2. Shear stress response (blue) to oscillations in normal stress (red) of amplitude $A = 2$ MPa and period $T = 5$ and 0.5 s. Note that “A” refers to the semi amplitude, 0-to-peak. Blue dotted line is initial, steady state shear stress. The parameter $\Delta\tau$ represents the frictional strength response and $\Delta\tau_{\text{yield}}$ is the difference between peak shear stress during normal stress oscillations and the initial shear stress. The phase lag between normal stress oscillation and the shear stress response is measured by $\Delta\phi$. Note that normal stress oscillations produce frictional weakening and thus the parameter $\Delta\tau_{\text{yield}}$ is negative.

Where, $t_{\text{on}}^{\text{max}}$ and t_{τ}^{max} are the time at the maximum of normal stress and shear stress, respectively.

All the parameters described above are calculated at the reference value of mean normal stress of 12.5 MPa.

4.2. Effect of Normal Stress Oscillations on Fault Frictional Response

As normal stress oscillations are imposed, the shear stress shows different responses depending on the amplitude and period of the oscillations. In general, we note three main responses. For periods, $T \leq 1$ s and amplitudes < 1 MPa, $\Delta\tau_{\text{yield}}$ is positive, with frictional strength greater than the initial steady state value, and the shear stress response is characterized by small amplitude and sporadic slow slip events (Figure 3a). For the same range of periods but higher amplitude of 2 MPa (Figure 3d), we observe an abrupt stress drop at the beginning of the oscillations, generally during the first time that normal stress decreases, after which the frictional strength remains well below the steady state value. Furthermore, we observe two superimposed responses of the shear strength. A short-term evolution where the shear stress oscillates almost in phase with the normal stress (i.e., Coulomb type response), and a long-term evolution where the shear stress accumulated during oscillations is released by fast (slip velocity of mm/s) (Figure 5f) and audible stress drops that take place just prior to, or when, the normal stress is at a minimum (Figure 3d). At intermediate periods and small amplitude ($T = 5$ s, $A = 0.5$ MPa, Figure 3b), slow slip events arise around the steady state shear strength, characterized by small stress drop and slow slip velocity. At the largest amplitude of 2 MPa and the same period of 5 s (Figure 3e), the first reduction in normal stress triggers an abrupt stress drop, which causes the frictional strength to decrease below the initial steady state value. Subsequent oscillations promote regular stick-slip events, characterized by larger stress drop and higher slip velocity (~ 1 mm/s), compared to the low amplitude cases. Common to both amplitudes investigated, at this period of oscillation, the shear stress is out of phase with normal stress, and the stress drops always take place close to the minimum in normal stress. At the longest period of 50 s, for all the amplitudes tested, we observe a Coulomb-type response of shear stress (Figures 3c and 3f). At this period, shear stress oscillates in phase with the normal stress around the mean value of the steady state strength. Note that for the largest amplitude of 2 MPa, during the descending phase of the normal stress we observe small slow-slip instabilities, that are suppressed during the ascending stage of normal stress loading. At the oscillation period of 10 s, we observe a transitional behavior between regular stick-slip, that we observe at 5 s, and a Coulomb-like response, that we observe at 50 s (Figure S4 in Supporting Information S1). This transient behavior, for all the amplitudes investigated, consists of complex, period doubling slip events (Figure S4 in Supporting Information S1).

It is interesting to note that for the cases with a frictional strength decrease ($A = 2$ MPa and $T \leq 5$ s), just after the normal stress oscillation is interrupted, the frictional strength comes back to steady state after ~ 100 μm of slip (~ 10 s) (see Figures 3d and 3e). When the frictional strength increases ($A = 0.5$ MPa and $T \leq 1$ s), the fault returns to steady state faster (~ 5 s, 50 μm of slip) (Figure 3a).

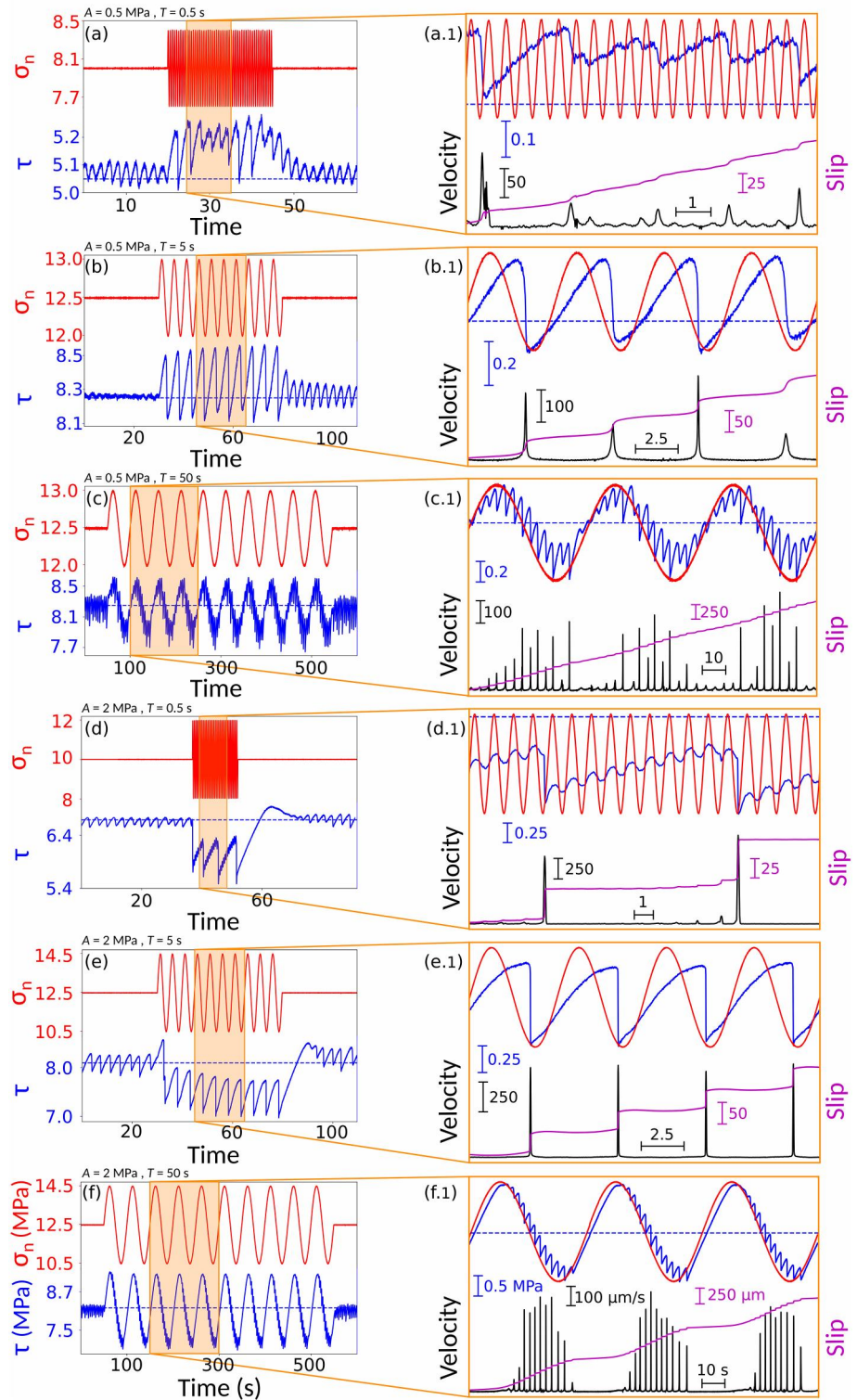


Figure 3. Mechanical data for a range of normal stress oscillations. Each panel shows the shear stress (blue) and normal stress (red) for one set of conditions. Blue dotted line shows the initial shear stress. Shaded areas in plots on left are shown as zooms on the right and include slip (magenta line) and slip velocity (black line) below the normal stress (A as on left) and shear stress (scale bar shown). (a) $A = 0.5$ MPa and $T = 0.5$ s (b) $A = 0.5$ MPa and $T = 5$ s (c) $A = 0.5$ MPa and $T = 50$ s (d) $A = 2$ MPa and $T = 0.5$ s (e) $A = 2$ MPa and $T = 5$ s (f) $A = 2$ MPa and $T = 50$ s. Note that small stress drops are observed during normal stress reduction for $T = 50$ s and more complex behavior, with large, dynamic slip events for other periods.

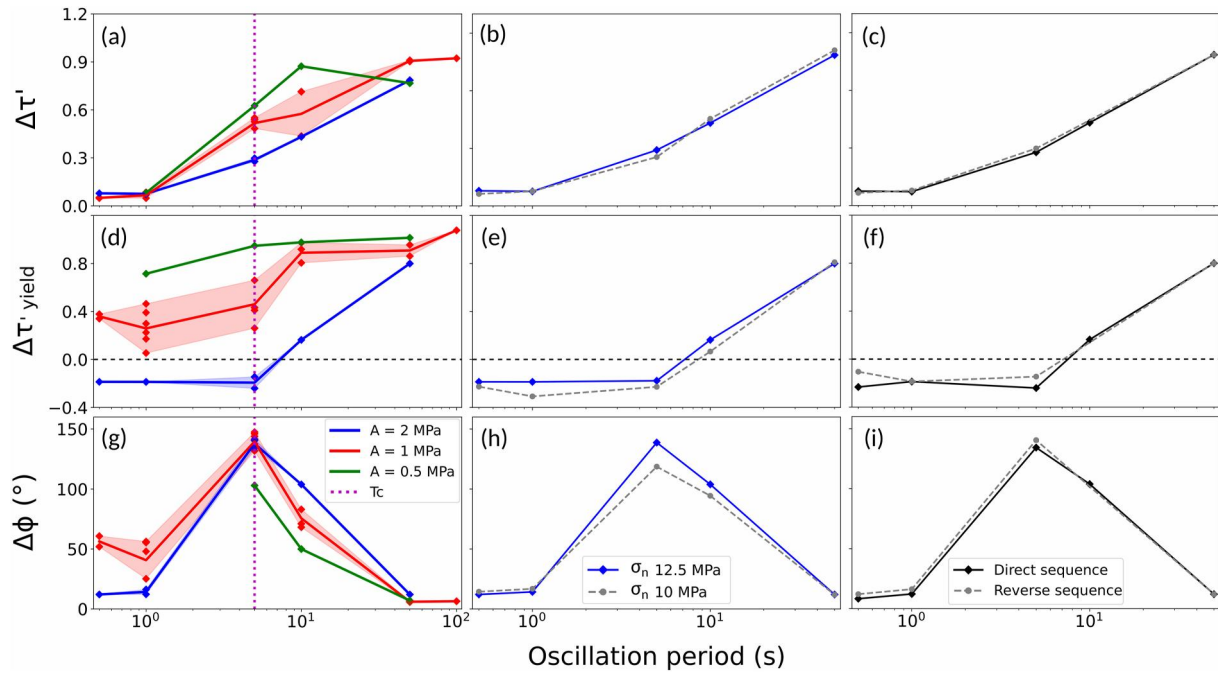


Figure 4. Effect of amplitude and oscillation period on frictional behavior. (a–c) Frictional strength variation, (d–f) peak yield strength variation, and (g–i) phase lag as a function of oscillation period. (left panel) Data for mean normal stress of 12.5 MPa. (center panels) Comparison of data for 12.5 and 10 MPa mean normal stress, both with $A = 2$ MPa. Data points correspond to averaged values for all tests. Lines are averages and the shaded area gives experimental variation. Magenta dashed line is the critical period ($T = 5$ s). Right panels compare data for our standard sequence (gray) to a reverse sequence with long periods first followed by short periods.

4.2.1. Frictional Strength Variation, $\Delta\tau'$

The normalized frictional strength variation $\Delta\tau'$ (Figure 2) represents the shear stress response to normal stress oscillations (Equation 10). This parameter can vary from values near 0, indicating that normal stress oscillations do not impact the shear stress, to values approaching 1, which implies an almost direct proportionality between normal stress and shear stress (i.e., Coulomb-like response resulting in nearly constant friction). At each oscillation amplitude, increasing the oscillation period from 0.5 to 50 s, the system varies from essentially no response of the shear stress to a Coulomb-like response.

At short periods, $T = 0.5$ and 1 s, $\Delta\tau'$ is close to zero for all the amplitudes investigated (Figures 4a–4c). As the period of oscillations increases, the values of $\Delta\tau'$ increases and approaches 1 at the longest periods. For periods $T > 1$ s, the amplitude of the normal stress oscillations has a systematic effect of decreasing $\Delta\tau'$ as the amplitude is increased. For example, at $T = 5$ s, $\Delta\tau'$ decreases from 0.3 to 0.6 as the oscillation amplitude decreases from 2 to 0.5 MPa.

4.2.2. Dynamic Weakening and Strengthening, $\Delta\tau'_{\text{yield}}$

The parameter $\Delta\tau'_{\text{yield}}$ is a measure of two different behaviors that are relevant for fault stability, that is, dynamic weakening and dynamic strengthening. Here, we define dynamic strengthening/weakening as the non-linear elastic softening/hardening observed in response to normal stress perturbations, consistent with the terminology used in previous studies (Boettcher & Marone, 2004; Hong & Marone, 2005; Richardson & Marone, 1999; Savage & Marone, 2008). Note that dynamic stressing is used here in contrast to static stresses. We define Dynamic weakening ($\Delta\tau'_{\text{yield}} < 0$) and this occurs when the fault slips at a lower strength as a consequence of normal stress oscillations (Figures 3d and 3e). Dynamic strengthening ($\Delta\tau'_{\text{yield}} > 0$) occurs when the fault slips at a higher strength as a consequence of normal stress oscillations (Figure 3a). Our results indicate that $\Delta\tau'_{\text{yield}}$ depends strongly on the period and amplitude of oscillation. This dependence on period increases as the oscillation amplitude increases. For short period oscillations, from $T = 0.5$ –5 s, large amplitudes cause dynamic weakening, with $\Delta\tau'_{\text{yield}} \sim -0.2$ (Figures 4d, 4e, and 4f). These are often associated with large and fast instabilities (Figures 3d and 3e). For the same periods, as the amplitude decreases, the fault undergoes dynamic

strengthening (~ 0.4 for $A = 1$ MPa and ~ 0.8 for $A = 0.5$ MPa) with instabilities that are much smaller and slower. As the oscillation period increases, up to the maximum of 50 s, $\Delta\tau_{\text{yield}'}$ is always positive, with values approaching unity regardless of the oscillation amplitude. To summarize, for most of the tested values of A and T , strengthening of the fault system occurred, and weakening took place only for $T < 5$ s and $A = 2$ MPa (Figures 4d–4f).

4.2.3. Phase Lag, $\Delta\varphi$

Understanding the evolution of phase lag between the imposed normal stress variations and the resulting shear stress response can give us important insight on the mechanics controlling frictional strength. The phase lag $\Delta\varphi$ is calculated from the oscillatory response of the shear stress during the inter-seismic period between slip events (Figures 2 and 3). Positive values of $\Delta\varphi$ indicate a delayed response in shear stress compared to the normal stress oscillations. For short period oscillations, $0.5 < T < 1$ s, we observe a fast response of shear stress to normal stress resulting in low values of $\Delta\varphi$ (Figure 4g). For $T = 5$ s we observe a peak in $\Delta\varphi$ up to values of 130° – 150° , corresponding to the maximum phase lag. As the period increases further, $\Delta\varphi$ gradually decreases, approaching values close to zero at the highest periods of oscillation (Figure 4g). It is interesting to note that this parameter shows a very weak dependency on the oscillation amplitude. Note that, $\Delta\varphi$ could not be calculated at $A = 0.5$ MPa and $T \leq 1$ s due to the lack of the oscillatory response.

4.2.4. Effect of Mean Normal Stress and Shear Strain

To ensure the validity of our observations, we tested the influence of shear strain and of small changes in mean normal stress. First, we describe the effect of the mean normal stress on the frictional response by choosing a $\sigma_n = 10$ and 12.5 MPa, which correspond to $k/k_c \sim 1$ (Table 1 and Figures 4b, 4e, and 4h). During these experiments we have imposed the same oscillation sequence and documented the evolution of $\Delta\tau'$, $\Delta\tau_{\text{yield}'}$ and $\Delta\varphi$. Our data show that, at a constant oscillation amplitude of $A = 2$ MPa, small variations in mean normal stress (and thus also of k/k_c) do not influence the frictional response of the fault gouge, which show the same trends as the reference case of $\sigma_n = 12.5$ MPa.

It is commonly accepted that shear localization and strain accommodation within a fault zone can influence the frictional behavior (e.g., Ikari et al., 2015; Logan et al., 1979; Noël et al., 2023; Rathbun & Marone, 2010). All of our experiments included two cycles of unloading-loading to promote shear localization. To interrogate the effect of strain localization on the shear stress response to normal stress oscillations, we performed an additional experiment at $\sigma_n = 12.5$ MPa and constant oscillation amplitude of 2 MPa with a reverse sequence of oscillation period (i.e., from high to low) (Figures 4c, 4f, and 4i). Comparing the calculated $\Delta\tau'$, $\Delta\tau_{\text{yield}'}$ and $\Delta\varphi$ with the standard oscillation sequence we see no difference between the two sequences. Thus, for the range of conditions we studied, shear strain, after reaching steady state sliding, does not have a strong effect on the frictional response.

4.2.5. Critical Period, T_c

For a fault subject to normal stress oscillations during shearing at constant loading rate, the critical period T_c corresponds to the time needed to accumulate enough slip to achieve a new steady state friction following a change in normal stress (Boettcher & Marone, 2004). Thus, at $T < T_c$ the shear zone never reaches a steady state and the system is continuously evolving. Combining the measurements of $\Delta\tau'$, $\Delta\tau_{\text{yield}'}$ and $\Delta\varphi$ we can determine the critical period at which the condition for resonance and destabilization should be favored under the elastic constraint of $k/k_c \sim 1$ following friction theory (e.g., Perfettini et al., 2001; Rice & Ruina, 1983).

Our data clearly show a strong dependence of all the above parameters on the vibration period. Combining data from Figures 4a, 4d, and 4g we can distinguish a critical period of 5 s, which seems to mark a common transition for all the parameters reported above (purple dashed line in Figures 4a, 4c, and 4d). At this period, and for all the tested amplitude, we observe: (a) a transition of $\Delta\tau'$ highlighting a transition from no to Coulomb-like response; (b) a transition of $\Delta\tau_{\text{yield}'}$ from a minimum to a maximum value; and (c) a clear peak in $\Delta\varphi$ showing a maximum out of phase response of the shear stress to the normal stress oscillations. It is important to note that the critical period of T_c is common for all the amplitudes tested across multiple experiments. Coupling our results between different stress, strain and amplitudes we consistently observe that the critical period for shear stress resonance is 5 s.

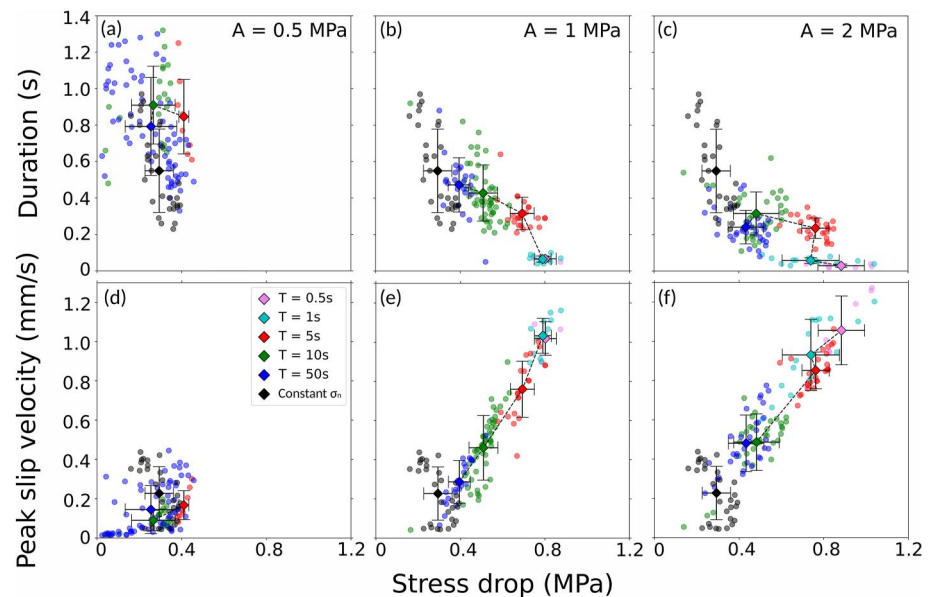


Figure 5. Slip event duration and peak slip velocity as a function of the stress drop for a range of amplitudes and periods. Colors correspond to oscillation period. Circles are single events while diamonds are mean values and standard deviation for each oscillation period. The black dots are the value computed at constant normal stress that is, between the normal stress oscillations. At oscillation amplitude of 0.5 MPa the points at 0.5 and 1 s of oscillation period are not reported because no systematic instability was recorded.

4.3. Slow and Fast Slip Instabilities Triggered by Normal Stress Oscillation

We also analyze the instabilities that arise during shearing under variable normal stress and compare them with the background slow-slips that we observe at constant normal stress to understand the triggering effect caused by normal stress oscillations. To characterize stick-slip instabilities we computed the stress drop, the peak slip velocity and slip duration (Figure S6 in Supporting Information S1). Note that here, for short oscillation periods ($T = 0.5$ and 1 s), we report the stress drop associated with the main event, which takes place after the fault has evolved over a number of oscillation cycles (Figure 3d and Figures S1 and S2 in Supporting Information S1).

We measure stress drop as the difference in shear stress before and after unstable slip events. In some cases, this coincides with the variation in frictional strength, $\Delta\tau$ (e.g., Figure 2; $T = 5$ s). For each stick-slip event, the slip velocity was obtained from the on-board LVDT. Thus, the fault slip velocities represent the average slip velocities across the fault zone. We determine velocity from displacement using a least square fit over a moving window of 0.03 s (i.e., 3 points). The peak slip velocity is the maximum slip velocity reached during each event (see Figure S6 in Supporting Information S1). The slip duration is the duration of the stress drop, that is, the time difference between the maximum and minimum in shear stress in correspondence of the stress drop.

At constant normal stress (i.e., $A = 0$ MPa) the system shows the typical slip behavior often observed at the bifurcation between the stable and unstable fields, with slow instabilities characterized by stress drop of about 0.3 MPa and peak slip velocity ranging between 100 and 400 $\mu\text{m/s}$, consistent with previous works (Figure 5) (e.g., Leeman et al., 2016; Scuderi et al., 2017). When the fault is perturbed by normal stress oscillations, the characteristics of the unstable events change depending on both the amplitude and the period of the oscillations (Figure 5). For small perturbation amplitude ($A = 0.5$ MPa) and short periods ($T = 0.5$ and 1 s), the system is characterized by aseismic creep with small acceleration but no reliable and repetitive slow or stick slip were recorded (Figures S1a and S2a in Supporting Information S1).

For the same small amplitude and periods $T > 1$ s, we observe unstable events characterized by long duration, stress drop between 0.3 and 0.4 MPa and peak velocity between 50 and 300 $\mu\text{m/s}$ (Figures 5a and 5d; Figures S3–S5 in Supporting Information S1). The variability of such events does not differ from the background instabilities and seem to be independent of oscillation period (Figures 5a and 5d).

In contrast, for higher amplitude perturbations ($A = 1$ and 2 MPa) we observe a strong control on event stress drop, duration and slip velocity, depending on the imposed normal stress oscillations (Figures 5b, 5c, 5e, and 5f). For periods T of 0.5 and 1 s (Figures S1 and S2 in Supporting Information S1), we observe fast (i.e., duration of a few milliseconds) and audible events with large stress drops of about 1 MPa and peak slip velocity that sometimes exceeds 1 mm/s (Figure 5). Note that here we report the major stress drop observed after several oscillations (e.g., Figure 2). At the critical period of $T_c = 5$ s and amplitude of 1 MPa (Figure S3 in Supporting Information S1) unstable events with a duration of ~ 0.3 s are characterized by stress drops of ~ 0.65 MPa and peak slip velocity of $V_{\text{peak}} \sim 750$ $\mu\text{m/s}$ (Figure 5). For amplitude of 2 MPa the unstable events are bigger (stress drop ~ 0.8 MPa), slightly faster (0.2 s), and result in higher peak slip velocity (850 $\mu\text{m/s}$). As the period of oscillation increases further ($T > 10$ s) (Figures S4 and S5 in Supporting Information S1), slow slip events during the unloading portion approach the values of duration, stress drop and slip velocity typical of the events at constant normal stress. For this range of amplitudes, depending on the oscillation frequency, we observe a spectrum of slip behaviors that ranges from slow to fast.

5. Discussion

Our observations show that stress perturbations can produce significant effects on frictional motion for a fault subject to loading conditions near the transition from stable to unstable behavior. For fault loading conditions near $k/k_c \sim 1$, normal stress oscillations near the critical period T_c can destabilize the fault and cause quasi-periodic or complex stick-slip sequences that are the laboratory equivalent of earthquakes. Moreover, the mechanical signature of laboratory earthquakes varies systematically with the amplitude and frequency of harmonic perturbations.

5.1. Rate and State Modeling and Parameters Choice

One simple question is the extent to which our laboratory data can be described by RSF. We use a forward model that solves the RSF friction constitutive equations with 1D elastic interaction and variable normal stress. We adopt a fifth order Runge-Kutta scheme to solve the numerical integration with an adaptive step-size control (following Boettcher & Marone, 2004). We use measured values of the RSF constitutive parameters derived from previous experiments on the same fault material and accounting for RSF evolution with shear strain (Scuderi et al., 2017). To account for uncertainties in parameter values, we studied a range of values for a and b from 0.01 to 0.021, varying a and b in steps of 0.005 with $b \geq a$, consistent with the experimental values. To simplify and reduce the number of variables, we decided to keep D_c fixed at 1.5 μm . For all the simulations performed, we used boundary conditions equal to those in the laboratory experiments: $V_{lp} = 10$ $\mu\text{m/s}$, $\sigma_n = 12.5$ MPa, $k' = 1.016 \times 10^{-3}$ μm^{-1} . For the parameter α (that represents the sensitivity to normal stress variation, Equation 6), we used values derived from additional experiments where instantaneous normal stress steps were performed (Figure S7 in Supporting Information S1). Those experiments show that α is ~ 0.26 , in agreement with previous work (Hong & Marone, 2005; Linker & Dieterich, 1992; Richardson & Marone, 1999; Shreedharan et al., 2019). To populate the range of periods investigated in the laboratory, simulations were performed at periods T of: 0.5, 1, 2, 3, 5, 7, 10, 25, 50, and 100 s, using the same amplitudes A performed in the laboratory experiments: 0.5, 1 and 2 MPa (see Figure S8 in Supporting Information S1). We computed results for each combination of a and b , corresponding to approximately 400 simulations for each set of amplitude and period. We assess data-model agreement using cross correlation between the laboratory data and model time series (Figure S9 in Supporting Information S1). Finally, the values of a and b with the highest correlation between the model and our laboratory data were selected for the model predictions discussed in the following paragraphs. The resulting parameters that best fit our laboratory data are given in the supplementary materials (see Table S1 in Supporting Information S1).

5.2. Model Prediction and Observations

RSF models with 1D elastic interaction reproduce the general mechanical evolution of the lab data reasonably well for both the Ruina and Dieterich state evolution laws (Figure 6). For short oscillation periods ($T = 0.5$ and 1 s), both evolution laws predict the long-term stick-slip behavior observed during the experiments with a short-term evolution of the shear stress that is in phase with the oscillations. However, the recurrence time between each stress drop and the magnitude of the stress drop depend on the evolution law. Ruina's law predicts a sudden stress drop that resets friction to a new state that remains lower than the initial strength. The peak stress levels and the

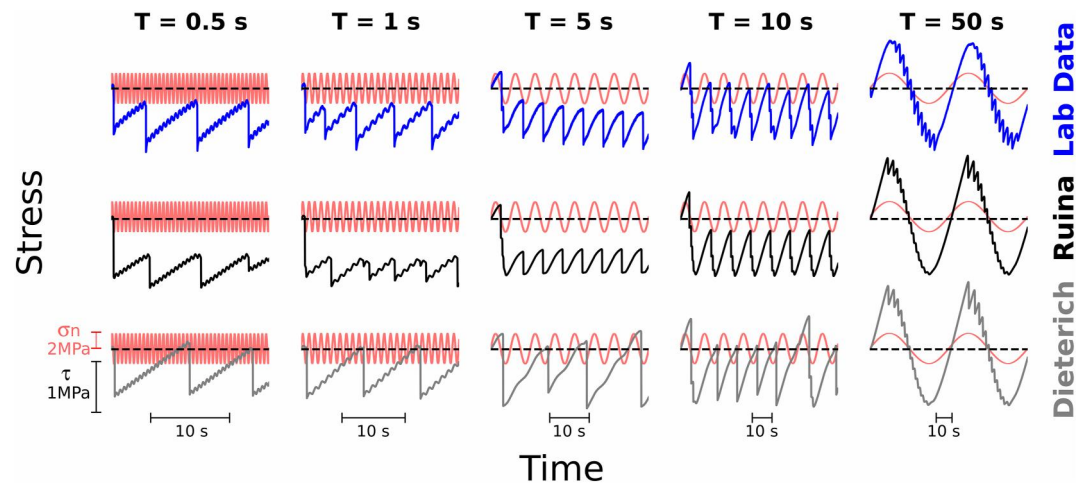


Figure 6. Comparison of laboratory data with rate and state friction model results for normal stress oscillations of $A = 2$ MPa. The red line is the normal stress and the blue, black and gray are respectively the shear stress of the lab data, Ruina's law and Dieterich's law. The black dashed line corresponds to the initial mean shear stress prior to oscillations and is the reference value for evaluation of dynamically induced weakening/strengthening. Note that the Ruina's law better predicts stress induced weakening and that both laws predict slip events and instability during times of normal stress decrease for $T = 50$ s however the lab data show larger instabilities at lower stress whereas the models predict the opposite.

predicted stress drops are lower than the lab observations (Figure 6). Dieterich's law predicts longer recurrence time and similar or larger stress drop magnitudes as the laboratory data. However, the peak values of shear stress are higher than the laboratory data (Figure 6).

At the critical period of $T_c = 5$, Ruina's law predicts dynamic weakening with regular stick-slip events that resemble in recurrence time and magnitude of the stress drop in the laboratory data (Figure 6). In contrast,

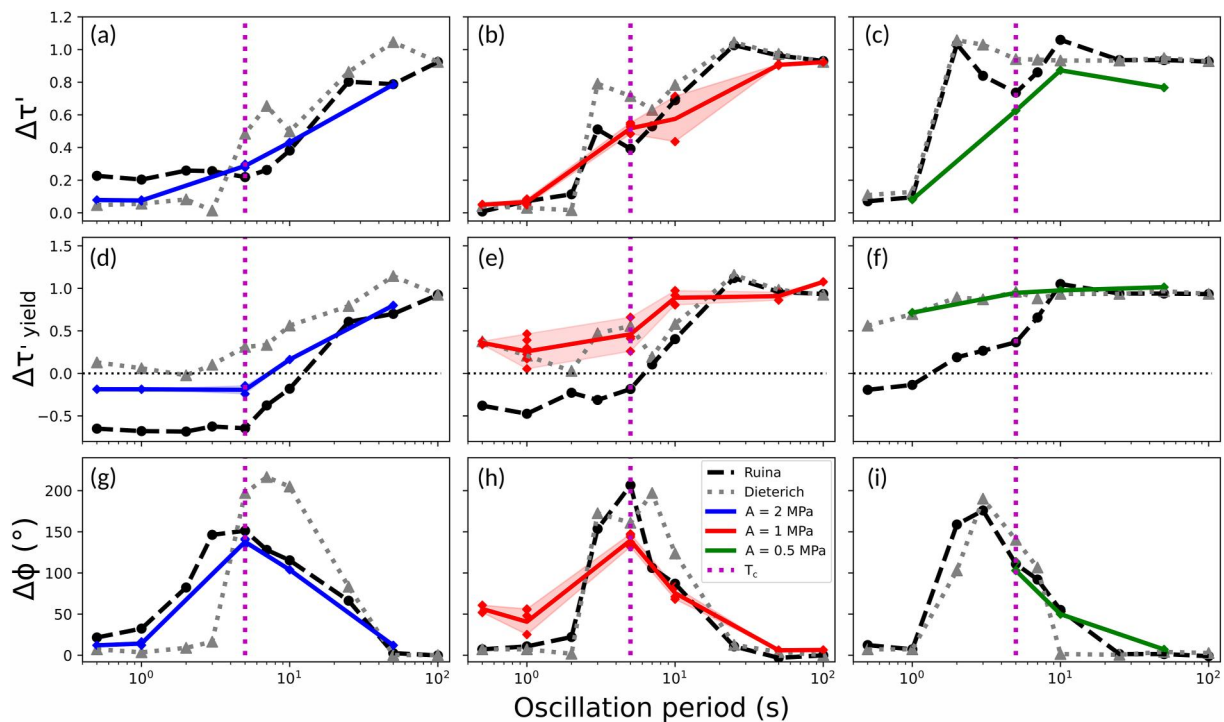


Figure 7. Comparison of lab data and rate and state friction model predictions of the parameters $\Delta\tau'$, $\Delta\tau'_{\text{yield}}$ and $\Delta\phi$ for a range of conditions (see legend in panel h). Blue/Red/Green lines are lab data. Black and gray dashed lines are Ruina and Dieterich's laws, respectively. Vertical magenta dashed line is the critical period defined on laboratory data. Note that the model predictions are in reasonable agreement with the laboratory data.

Dieterich's law predictions do not match well the experimental data, with longer recurrence times and larger stress drops than the experimental data. For normal stress oscillations of $T = 10$ s both evolution laws match the general behavior observed, with periodic lab-quakes and a hint of period doubling shown by smaller stress drops superimposed on the larger periodic events (Figure 6). Also in this case, Ruina's law better resembles the laboratory observations. At $T = 50$ s, both evolution laws are generally consistent with our data, with a quasi-linear increase of the shear stress during the normal stress loading and small instabilities of variable stress drop during the normal stress decrease. Both laws predict small amplitude lab-quakes during higher shear stress, in contrast to the laboratory data (Figure 6).

To evaluate the consistency of the RSF models with our laboratory data, we computed the parameters $\Delta\tau'$, $\Delta\tau_{\text{yield}}'$ and $\Delta\phi$ from the calculated shear stress, for each amplitude and period tested (Figure 7). Results for both evolution laws are in general agreement with our measured parameters, showing very similar trends. Both the evolution laws well predict $\Delta\tau'$, with the exception that Dieterich's law tends to overestimate the experimental values around T_c . The evolution laws differ the most on the prediction of $\Delta\tau_{\text{yield}}'$. Ruina's law always predicts dynamic weakening at oscillation period shorter than T_c and for all the amplitudes, while in the laboratory data there is a dynamic weakening only at oscillation amplitude of 2 MPa. Dieterich's law always predicts dynamic strengthening that is inconsistent with experimental data at $A = 2$ MPa (Figure 7d). Common to all models and experimental data, the phase lag ($\Delta\phi$) shows a peak around the critical period (T_c) (Figures 7g and 7h).

From the model outputs and using the lab RSF parameters, Ruina's evolution law is more consistent with the laboratory data, especially for $T_c = 5$ s. To quantify which evolution law is more representative of the experimental data, we compute the correlation coefficient between the curves shown in Figure 7 (details in Figure S9 in Supporting Information S1). For $\Delta\phi$ and $\Delta\tau_{\text{yield}}'$ the correlation coefficient is always higher for Ruina's evolution law, while for $\Delta\tau'$ at oscillation amplitude of 0.5 and 2 MPa is higher for Dieterich, but in both cases is very high (>0.86).

Based on the correlation coefficient, for the frictional parameters used in this modeling, Ruina's evolution law better represents the laboratory data. It is worth noting that the same RSF models applied to instantaneous normal stress steps on granite bare surfaces (Shreedharan et al., 2019) also demonstrate that the friction evolution in response to stress perturbation is better fitted by the Ruina Slip law. However, we note that our model results were calculated for a single value of D_c . Future work is needed to explore the impact of D_c on model predictions.

5.3. Previous Works on Stress Perturbation Experiments

In laboratory settings, the response of faults to external normal stress perturbations is primarily investigated by varying the normal stress using two approaches: (a) performing instantaneous up and down steps and (b) sinusoidal oscillations. Previous experiments, where normal stress steps were performed on bare rock surfaces, have extensively documented that shear strength increases as a result of instantaneous up-steps (Kilgore et al., 2012, 2017; Linker & Dieterich, 1992; Shreedharan et al., 2019). These studies convincingly demonstrate, through the integration of mechanical data with the recording of ultrasonic wave amplitude, that the observed variation in shear strength is related to changes in the real contact area at the micro-scale of asperity contacts (Shreedharan et al., 2019).

For quartz fault gouge, a similar strength evolution in response to instantaneous normal stress steps has been observed and interpreted as originated by the evolution of contact area at grain contact (Hong & Marone, 2005; Richardson & Marone, 1999). We note that our normal stress step experiments (Figure S7 in Supporting Information S1) are in agreement with Hong and Marone (2005), providing comparable values of α for quartz gouge under 100% humidity conditions. This is true even if the mean grain size of the fault gouge was one order of magnitude different.

Vibration experiments (i.e., high frequency-high amplitude) on quartz fault gouge during stationary contact of slide-hold-slide experiments have shown that the shear strength upon re-shearing increases as a function of vibration amplitude (Frye & Marone, 2002; Richardson & Marone, 1999). This observation highlights that vibration can increase contact quality and/or quantity enhancing frictional healing.

Experiments on quartz fault gouge, where the amplitude and frequency of normal stress oscillations were systematically varied, show that high amplitude and short period perturbations cause dynamic weakening, associated

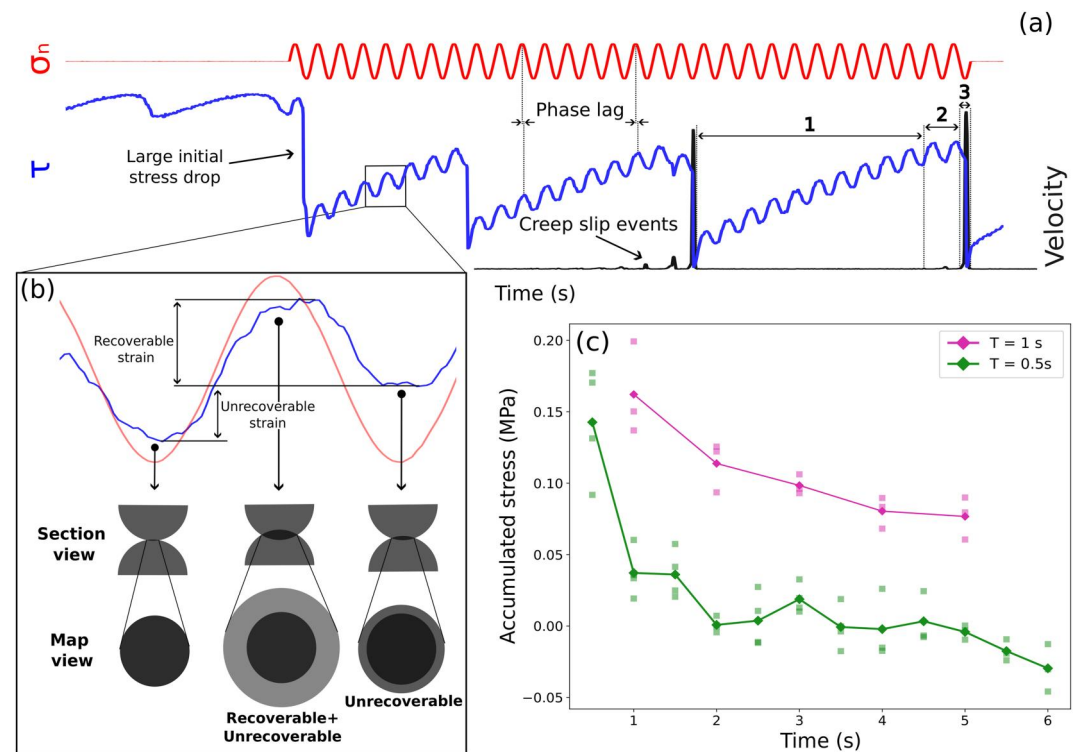


Figure 8. Data and schematic interpretation of frictional response to normal stress oscillations. Panel (a) shows the evolution of shear stress (blue) in response to normal stress oscillations (red) of $A = 2$ MPa and $T = 0.5$ s. Black line at bottom shows the fault slip velocity. Note that normal shear and shear stress are almost in phase. The numbers (1–3) refer to the three different stages discussed in the text. Panel (b) is a zoom of one normal stress oscillation from (a) with the recoverable and unrecoverable normal strain. Lower part of (b) shows micro-mechanical evolution of the contacts during stress oscillations. (c) Evolution of the accumulated stress used to evaluate the unrecoverable normal strain in time (i.e., number of oscillations).

with an initial large stress drop at the beginning of the perturbation (Boettcher & Marone, 2004). As the amplitude of oscillation is decreased, the fault seems to be not affected by the perturbation and slides at the frictional steady state. At longer periods, independently of the amplitude of oscillations the fault shows a Coulomb like response. Similar to our data they show that a required condition to induce dynamic weakening and potentially destabilize a creeping fault is a large stress drop at the beginning of the perturbation. Boettcher and Marone suggested that the initial stress drop causes rejuvenation of the asperity population, that is, $\theta = \theta_0$, that can evolve and grow during the following perturbation, however, remaining lower when compared to steady state friction at constant normal stress. However, they did not document consistent stick-slip behavior, as predicted by the analytical solution of Perfettini et al. (2001), because the high stiffness of the apparatus they used, which was well above the critical stiffness of the fault gouge. In the current study we build on these observations and show that when the $k/k_c \sim 1$ a creeping fault can be destabilized, resulting in a spectrum of slip behaviors.

5.4. Short Period Perturbations ($T = 0.1 T_c$)

At oscillation amplitudes of 1 and 2 MPa, the fault responds by dynamically weakening, with a major initial stress drop induced during the first oscillation (Figures 3 and 4). Afterward, fault strength always remains lower than the steady state and evolves in phase with the normal stress oscillations (Figure 4g), for a number of cycles until the occurrence of a seismic event. This behavior is common for all the experiments and simulations under our boundary conditions. However, the origin of this behavior is counterintuitive since it shows the superimposition of two mechanical effects: (a) a Coulomb like response where frictional strength proportionally increases/decreases with normal stress, and (b) a strain hardening loading that allows the fault to accumulate elastic energy to be released in a stress drop after a certain number of cycles. The coupling of these two observations shows that at high frequency and high amplitude of oscillation the fault experiences delayed dynamic triggering and can generate seismic stress drops (Figure 5).

To find the micro-mechanical origin of the observed behavior, we propose that, the high perturbation stress rate, given by a large change in stress in a short time window, is able to generate an initial large stress drop that resets the fault state with the resulting creation of a new population of young contacts (Figure 8a) (e.g., Boettcher & Marone, 2004). Following the first half period oscillation, in response to normal stress increase these young frictional contacts strengthen and increase fault state, based on RSF laws (Equation 7). As the normal stress begins to decrease, part of the elastic normal strain that has been accumulated is released, causing a proportional decrease in strength, as expected for a simple Coulomb-like response. Indeed, our calculation of the phase shift (Figures 4g–4i) and the results from the models (Figure 7) show that for these short perturbation periods the phase lag is always close to zero suggesting a Coulomb-like response. However, our observations show that part of the normal strain accumulated during loading is permanently stored, resulting in an incremental accumulation in shear strength for each normal stress cycle (Figure 8b). A plausible mechanism to allow shear strength to increase is that deformation at contacts junctions is partitioned between recoverable and unrecoverable normal strain, causing the “quality” of the contacts to increase (i.e., contact area and strength grow permanently) at each oscillation cycle (Figure 8b) (Kilgore et al., 2017; Shreedharan et al., 2019). We quantify this effect by calculating the difference between the changes in strength during the loading and unloading portion of the normal stress cycle, as detailed below, in order to evaluate the unrecoverable normal strain stored during the oscillations (Figures 8b and 8c).

Following a major stress drop, we can describe the evolution of fault strength during a seismic cycle in three main stages (Figure 8a). During stage one, the fault is locked (Figure 8a, Figure S1c in Supporting Information S1) and is characterized by a young (and small proportional to applied mean normal stress) population of contacts that have the capability to grow. In response to the normal stress oscillation, the fault is more efficiently locked, while the constant remote loading rate transfers stress to the fault, resulting in a stress accumulation during each cycle of normal stress oscillations (Figure 8b). During this phase, the population of contacts increases in quality resulting in an increase in shear strength, allowing the storage of elastic energy.

During stage two the fault is in a high stress state with contacts that are approaching the maximum size for the accumulated stress (Figure 8c). This observation is valid for both the short oscillation periods ($T = 1$ and 0.5 s) where we observe a progressive decrease of stress accumulation up to a plateau with time (i.e., number of oscillations) (Figure 8c). During late stage two, the fault has reached his maximum strength and the contacts have reached a critical size, causing a plateau in shear strength, resulting in the onset of small creep events (i.e., acceleration of slip in Figure 8a). Finally, in stage three the contacts cannot continue to strengthen and the fault begins to unlock and slip causing a seismic stress drop (where energy radiation was audible) at velocity >1 mm/s (Figure 5f).

Our micromechanical interpretation aligns with the one of Shreedharan et al. (2019). By analyzing the variation in P -wave velocity, Shreedharan et al. (2019) suggests an enhancement in the quality and quantity of contacts in response to an increase in normal stress. In their interpretation, an immediate increase in P -wave velocity occurs upon imposing an increase in normal stress, attributable to the elastic increase of real contact area. This elastic portion corresponds to our recoverable strain, while the unrecoverable strain is attributable to the further inelastic growth of the contact junction observed after the immediate P -wave velocity.

It is important to note that to reach the critical condition and generate a seismic event the number of the oscillations for $T = 0.5$ s is approximately doubled respect to $T = 1$ s resulting in a common recurrence time of ~ 5 s (Figure S10 in Supporting Information S1). This observation implies that we can interpret the contact evolution as a time dependent process rather than a slip dependent process.

Our conceptual interpretation in terms of contact mechanics is coherent with the dynamic strengthening observed at low amplitude. Under these perturbation conditions, we never observe the initial seismic stress drop that is a requirement to reset the state of the fault and create a young and smaller contact population. Instead, the normal stress oscillation perturbs the existing “old” contact population established at constant normal stress. It results that the perturbation enhances contact growth, causing shear strength to increase above the steady state (i.e., positive $\Delta\tau_{\text{yield}}$). It results that the fault creeps, with some accelerations, at higher shear strength and never experiences stick slip behavior causing further growth, resulting in dynamic strengthening of the fault.

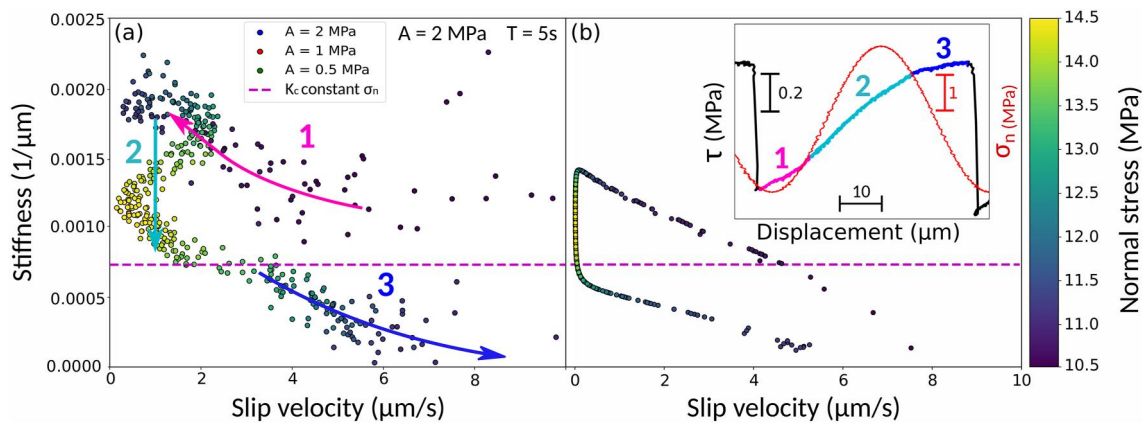


Figure 9. Comparison of the loading stiffness as function of the slip velocity for lab data (a) and the rate and state friction model (b). Stiffness is calculated as the slope of the shear stress-displacement curve in the inter-seismic phase (see inset in the top right). The magenta dashed lines show k_c calculated with the friction parameter at constant normal stress. The inset in panel (b) show the three different trends for the entire stick slip cycle.

5.5. Critical Perturbation Period ($T = T_c$)

At the critical period $T = 5$ s, when the fault is perturbed at high oscillation amplitude, a regular stick-slip behavior is observed that is out of phase with the normal stress perturbations (Figures 3b and 3e). This behavior is clear at $A = 1$ and 2 MPa, while at $A = 0.5$ MPa the slip behavior remains slow (Figure 5). As observed for the short period and large amplitude oscillation (Section 5.6), the onset of the normal stress perturbation causes a large stress drop that reset fault state and causes dynamic weakening with shear stress that always remains below the steady state (Boettcher & Marone, 2004).

To shed light on the origin of regular instability during normal stress perturbation and compare with the theoretical framework of RSF we measure the evolution of fault stiffness during the inter-event time. Our goal is to map the evolution of the fault stiffness during each perturbation to find a relation with the experimentally derived fault critical stiffness (k_c) to verify if instabilities correspond to the critical stability condition, $k/k_c < 1$. For this purpose, during the perturbation, we compute the slope of the shear stress as a function of shear displacement over a small moving window of 0.1 s during the inter-seismic stage.

Our analysis shows that stick slip cycles can be divided into three stages (Figure 9a). Stage one is characterized by a post seismic deceleration and an increase in fault stiffness. We suggest that this corresponds to a new and young contact population that is packing into a new configuration. During stage two the fault is locked, and slip velocity remains much lower than the background loading rate of 10 $\mu\text{m/s}$ (Figure 9a and Figure S11 in Supporting Information S1). During this stage contact growth could be the cause of increased shear strength and elastic energy accumulation. The combined action of remote loading rate and increasing normal stress causes stiffness to decrease due to an increase in contact area until the peak in normal stress. During stage three, as the fault approaches the critical stiffness and the stiffness ratio is ~ 1 , fault slip begins to accelerate until the nucleation of an instability.

The model (Ruina) is consistent with stiffness and slip evolution during the normal stress perturbations observed in the experiments at the critical period for all the oscillation amplitude (Figure 9b), suggesting that slip is required for contact evolution. Our experimental results and model output are fully consistent with the predictions of RSF laws. That is, to nucleate an instability, under this condition, the stability parameter k/k_c must be less than 1 as also proposed by previous theoretical work (Perfettini et al., 2001).

5.6. Long Perturbation Period ($T = 10T_c$)

At long oscillation period the system response to oscillation can be described by a Coulomb-like behavior. To understand the stability of the system during this oscillation period we measure the stiffness (with the same method used at the critical period). The low amplitude perturbation does not change the slow slip behavior present at constant normal stress. This means that the perturbation is slow enough to allow the contacts to evolve

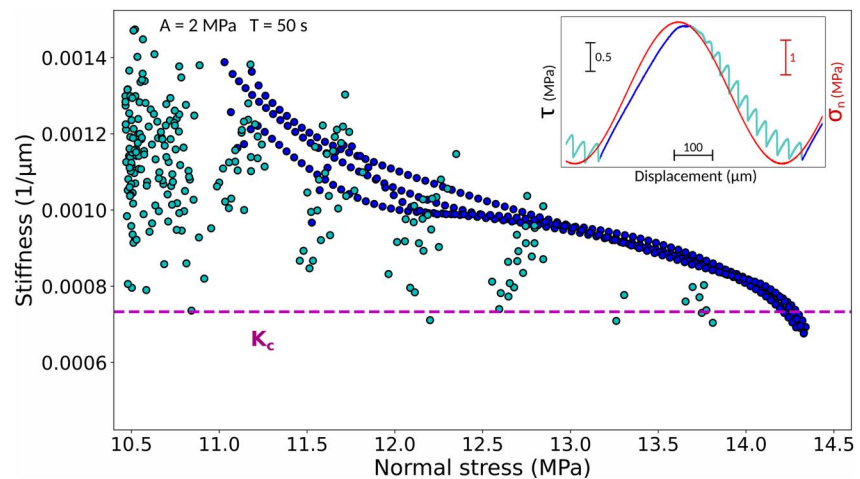


Figure 10. Stiffness evolution during the normal stress perturbation at $A = 2$ MPa and $T = 50$ s. The blue points correspond to the stiffness calculated during the normal stress increase; the cyan points correspond to the stiffness calculated at the loading portion of the events during the normal stress decrease. The colors used in the main panel are also used in the inset. The magenta dashed lines represent the rheological critical stiffness, k_c , calculated with the friction parameters at constant normal stress.

simultaneously with the perturbation in normal stress. In other words, the fault has time to adapt to the ever-changing condition.

At large oscillation amplitude ($A = 2$ MPa) the fault is locked during the normal stress increase (Figure 3) and the shear strength linearly and elastically increases (portion 1 inset in Figure 10). As observed for the case at the critical period, stiffness decreases during this stage. To note that at the peak in normal stress the stiffness of the system remains around the critical fault rheologic stiffness. As the normal stress begins to decrease (portion 2 inset in Figure 10) small slow instabilities spontaneously arise (peak slip velocity ~ 400 $\mu\text{m/s}$, Figure 5f). Stiffness during the inter-seismic stage of the slow stick-slip remain around or above the critical stiffness consistently with the RSF theory.

6. Implications for Natural Faults

The dynamic triggering of earthquakes is a complex and challenging phenomenon in earthquake mechanics due to its ability to occur with a considerable time delay and over long distances from the triggering source (Freed, 2005; Shelly et al., 2011). While there have been several documented cases of dynamic triggering in nature, many of these have been observed in geological settings characterized by fluid overpressure, such as geothermal environments or regions where fluid injection is performed (Gomberg & Bodin, 1994; Gomberg & Davis, 1996; Van der Elst et al., 2013). Additionally, dynamic triggering has been noted in extensional settings like oceanic ridges (Scholz et al., 2019). These observations consistently reveal that the normal stress in these settings is particularly low, resulting in a significant effective perturbation.

Our results suggest that specific stress perturbation can promote fault slip and generate seismicity. Indeed, in some cases it has been shown that tectonic tremors (Beroza & Ide, 2011; Gomberg et al., 2010) are related to tidal modulation and low frequency waves (Ide, 2010; Miyazawa & Mori, 2006; Peng & Chao, 2008; Rubinstein et al., 2007; Shelly et al., 2007). Moreover external dynamic perturbations may represent a triggering mechanism for slow earthquakes that in some cases have been found to be related to the nucleation of large megathrust earthquakes (Cruz-Atienza et al., 2021; Kato et al., 2012; Obara & Kato, 2016).

In terms of perturbation frequency, most of the previous studies (Gomberg & Davis, 1996) have agreed on the fact that high-frequency perturbations are more effective at triggering earthquake compared to low-frequencies perturbations (Beeler & Lockner, 2003; Scholz, 2003; Vidale et al., 1998). Moreover, Gomberg et al. (2003, 2004) show how the triggered seismicity is distributed along the rupture's directivity of the main shock that generates the transient perturbation. Indeed, accounting for rupture directivity shows how the seismic energy propagation causes stronger dynamic stressing. This observation is consistent with our results, which show that

higher perturbation stresses (i.e., high amplitude, low period up to the critical period) are most effective in generating dynamic triggering.

Our laboratory data also show that different perturbations can strongly change the slip behavior of a fault depending on the amplitude and frequency. Based on our own experimental results and in agreement with most of the natural observations of dynamic earthquake triggering, we propose three essential conditions for an external perturbation to effectively trigger an instability:

1. The perturbation stress must exhibit a high effective amplitude.
2. The period of the perturbation must be short, preferably equal to or shorter than the critical friction period.
3. The duration of the perturbation must be at least as long as the critical period.

The first two points are key for producing the high stressing rates required to trigger instability. To attempt a comparison between our laboratory experiments and natural observations we can use Equation 8 and estimate the critical period in natural settings following the same approach of Boettcher and Marone (2004).

Assuming a plate rate velocity of 30 mm/year and using rate and state parameters derived from laboratory studies on the same material under similar boundary conditions ($a = 0.015$, $b = 0.0161$; Scuderi et al., 2017), the critical period, T_c , strongly varies depending on the value of D_c . In laboratory studies, D_c is of the order of micrometers, resulting in a T_c of approximately 10 hr. In natural settings, we can assume a D_c of 1.5 mm (Marone & Kilgore, 1993; Marone et al., 2009), leading to a critical period of around 1 year. Consequently, using a D_c on the order of centimeters, T_c is on the order of a decade.

What are the natural phenomena that could result in stress variations with periods smaller than or equal to 1 year?

1. Seismic body wave frequencies typically range from 1 to 100 Hz, while surface waves range from 0.1 to 1 Hz (Lei & Ma, 2014). Seismic waves tend to attenuate over distance; therefore, we can anticipate that a dynamic triggering effect is more efficient when closer to the perturbation source. Moreover, since surface waves have greater amplitudes relative to body waves and exhibit less attenuation over distance, we can expect that surface waves potentially have a more significant triggering effect. Thus, seismic waves represent high perturbation frequencies, potentially with high amplitudes, suggesting that they can act as triggering sources.
2. Earth tidal loading periods are in the order of hours. In some cases, it has been found to correlate with an increase in seismicity rate (Beauc e et al., 2023; Cochran et al., 2004; Scholz et al., 2019). However, frequently, the correlation between seismicity and Earth tides is observed for shallow faults, indicating that they may require a low fault-normal load, meaning a higher perturbation effective amplitude.
3. Climatic-induced stress cycles (e.g., seasonal hydrology, seasonal accumulation and thaw of ice cover, etc.) are characterized by periods of about 1 year. Periodic slow slips have been observed to correlate with these climate-induced stress changes, suggesting that the periodicity of slow slip may be due to a resonance effect (Lowry, 2006).

The understanding that dynamic earthquake triggering can take place beyond regions with high seismicity rates (Brodsky et al., 2000; Gomberg et al., 2004) and that faults may be critically stressed elsewhere (Townend & Zoback, 2000), makes it challenging to understand the areas most prone to being triggered. Therefore, experimental and natural observations highlight, for an earthquake triggering, the importance of the properties of the perturbation and its interaction with the fault and its surrounding.

7. Conclusions

Laboratory friction experiments under critical stiffness condition show that normal stress perturbations control the slip behavior of the fault and act as earthquake triggering depending on the amplitude and period of the oscillation. Starting from a slow slip behavior, typical of the critical stiffness condition, low oscillation amplitude and short oscillation period strengthen the fault, suppressing the slow slip instabilities and generating a creep slip with some accelerations. In contrast, high oscillation amplitude and short period weaken the fault enhancing an unstable slip behavior. At high oscillation period the fault is modulated by the normal stress oscillation resulting in Coulomb-like response. At the critical oscillation period ($T = 5 s = T_c$) the slip behavior clearly becomes unstable with regular fast stick slip. Moreover, at this perturbation period, the evolution of the stiffness during the oscillation shows fault acceleration when k becomes smaller than k_c , that is, when the fault enters the unstable field. Depending on normal stress oscillation amplitude and period we can clearly see a transition from slow to

fast slip events. Using rate and state modeling, we demonstrated that both Ruina and Dieterich evolution laws predict the observed experimentally behaviors, with Ruina's law that is more consistent with the experimental data. Our findings shed light on the effects of stress changes on fault strength and slip behavior, with important implications for earthquake hazard assessment.

Data Availability Statement

The collected data and the Python scripts implemented in this paper are available at Pignalberi et al. (2023), <https://doi.org/10.5281/zenodo.8131061>. For any further request, please don't hesitate to contact the corresponding author at federico.pignalberi@uniroma1.it.

Acknowledgments

The authors thank the Editor Satoshi Ide, the Associate Editor, Brian Kilgore, and an anonymous reviewer for their constructive comments that improved the manuscript. This research was funded by European Research Council ERC g.a. no. 835012 (TECTONIC) to CM, ERC g.a. n.o. 101040600 (HYQUAKE) to MMS, PRIN giovani PREVENT to MMS and, Marie Skłodowska-Curie Action g.a. n.o. 101065365 (SHEAR) to CG. CM also acknowledges support from RETURN Extended Partnership and received funding from the European Union Next-GenerationEU (National Recovery and Resilience Plan—NRRP, Mission 4, Component 2, Investment 1.3—D.D. 1243 2/8/2022, PE0000005) and US Department of Energy projects DE-SC0020512 and DE-EE0008763.

References

- Baumberger, T., Heslot, F., & Perrin, B. (1994). Crossover from creep to inertial motion in friction dynamics. *Nature*, *367*(6463), 544–546. <https://doi.org/10.1038/367544a0>
- Beaucé, E., Poli, P., Waldhauser, F., Holtzman, B., & Scholz, C. (2023). Enhanced tidal sensitivity of seismicity before the 2019 magnitude 7.1 Ridgecrest, California earthquake. *Geophysical Research Letters*, *50*(14), e2023GL104375. <https://doi.org/10.1029/2023GL104375>
- Bedford, J. D., & Faulkner, D. R. (2021). The role of grain size and effective normal stress on localization and the frictional stability of simulated quartz gouge. *Geophysical Research Letters*, *48*(7), e2020GL092023. <https://doi.org/10.1029/2020GL092023>
- Beeler, N. M., & Lockner, D. A. (2003). Why earthquakes correlate weakly with the solid Earth tides: Effects of periodic stress on the rate and probability of earthquake occurrence. *Journal of Geophysical Research*, *108*(B8), 2391. <https://doi.org/10.1029/2001JB001518>
- Beroza, G. C., & Ide, S. (2011). Slow earthquakes and nonvolcanic tremor. *Annual review of Earth and planetary sciences*, *39*(1), 271–296. <https://doi.org/10.1146/annurev-earth-040809-152531>
- Bettinelli, P., Avouac, J.-P., Flouzat, M., Bollinger, L., Ramillien, G., Rajaura, S., & Sapkota, S. (2008). Seasonal variations of seismicity and geodetic strain in the Himalaya induced by surface hydrology. *Earth and Planetary Science Letters*, *266*(3–4), 332–344. <https://doi.org/10.1016/j.epsl.2007.11.021>
- Boettcher, M. S., & Marone, C. (2004). Effects of normal stress variation on the strength and stability of creeping faults. *Journal of Geophysical Research*, *109*(B3), B03406. <https://doi.org/10.1029/2003JB002824>
- Brodsky, E. E., Karakostas, V., & Kanamori, H. (2000). A new observation of dynamically triggered regional seismicity: Earthquakes in Greece following the August 1999 Izmit, Turkey earthquake. *Geophysical Research Letters*, *27*(17), 2741–2744. <https://doi.org/10.1029/2000GL011534>
- Chanard, K., Nicolas, A., Hatano, T., Petrelis, F., Latour, S., Vinciguerra, S., & Schubnel, A. (2019). Sensitivity of acoustic emission triggering to small pore pressure cycling perturbations during brittle creep. *Geophysical Research Letters*, *46*(13), 7414–7423. <https://doi.org/10.1029/2019GL082093>
- Cochran, E. S., Vidale, J. E., & Tanaka, S. (2004). Earth tides can trigger shallow thrust fault earthquakes. *Science*, *306*(5699), 1164–1166. <https://doi.org/10.1126/science.1103961>
- Colletini, C., Di Stefano, G., Carpenter, B., Scarlato, P., Tesei, T., Mollo, S., et al. (2014). A novel and versatile apparatus for brittle rock deformation. *International Journal of Rock Mechanics and Mining Sciences*, *66*, 114–123. <https://doi.org/10.1016/j.ijmms.2013.12.005>
- Cruz-Atienza, V. M. V. M., Tago, J., Villafuerte, C., Wei, M., Garza-Girón, R., Dominguez, L. A., et al. (2021). Short-term interaction between silent and devastating earthquakes in Mexico. *Nature communications*, *12*(1), 2171. <https://doi.org/10.1038/s41467-021-22326-6>
- Dieterich, J., Cayol, V., & Okubo, P. (2000). The use of earthquake rate changes as a stress meter at Kilauea volcano. *Nature*, *408*(6811), 457–460. <https://doi.org/10.1038/35044054>
- Dieterich, J. H. (1979). Modeling of rock friction: 1. Experimental results and constitutive equations. *Journal of Geophysical Research*, *84*(B5), 2161–2168. <https://doi.org/10.1029/JB084iB05p02161>
- Dieterich, J. H. (1981). Constitutive properties of faults with simulated gouge. In *Mechanical behavior of crustal rocks* (pp. 103–120). American Geophysical Union (AGU). <https://doi.org/10.1029/GM024p0103>
- Dieterich, J. H., & Linker, M. F. (1992). Fault stability under conditions of variable normal stress. *Geophysical Research Letters*, *19*(16), 1691–1694. <https://doi.org/10.1029/92GL01821>
- Ellsworth, W. L. (2013). Injection-induced earthquakes. *Science*, *341*(6142), 1225942. <https://doi.org/10.1126/science.1225942>
- Ellsworth, W. L., & Bulut, F. (2018). Nucleation of the 1999 Izmit earthquake by a triggered cascade of foreshocks. *Nature Geoscience*, *11*(7), 531–535. <https://doi.org/10.1038/s41561-018-0145-1>
- Freed, A. M. (2005). Earthquake triggering by static, dynamic, and postseismic stress transfer. *Annual Review of Earth and Planetary Sciences*, *33*(1), 335–367. <https://doi.org/10.1146/annurev.earth.33.092203.122505>
- Frye, K. M., & Marone, C. (2002). Effect of humidity on granular friction at room temperature. *Journal of Geophysical Research*, *107*(B11), ETG-11. <https://doi.org/10.1029/2001JB000654>
- Gomberg, J., Beeler, N. M., Blanpied, M. L., & Bodin, P. (1998). Earthquake triggering by transient and static deformations. *Journal of Geophysical Research*, *103*(B10), 24411–24426. <https://doi.org/10.1029/98JB01125>
- Gomberg, J., Blanpied, M. L., & Beeler, N. M. (1997). Transient triggering of near and distant earthquakes. *Bulletin of the Seismological Society of America*, *87*(2), 294–309. <https://doi.org/10.1785/BSSA0870020294>
- Gomberg, J., & Bodin, P. (1994). Triggering of the Ms = 5.4 Little Skull Mountain, Nevada, earthquake with dynamic strains. *Bulletin of the Seismological Society of America*, *84*(3), 844–853. <https://doi.org/10.1785/BSSA0840030844>
- Gomberg, J., Bodin, P., Larson, K., & Dragert, H. (2004). Earthquake nucleation by transient deformations caused by the M = 7.9 Denali, Alaska, earthquake. *Nature*, *427*(6975), 621–624. <https://doi.org/10.1038/nature02335>
- Gomberg, J., Bodin, P., & Reasenber, P. A. (2003). Observing earthquakes triggered in the near field by dynamic deformations. *Bulletin of the Seismological Society of America*, *93*(1), 118–138. <https://doi.org/10.1785/0120020075>
- Gomberg, J., Cascadia 2007, & Beyond Working Group. (2010). Slow-slip phenomena in Cascadia from 2007 and beyond: A review. *Bulletin*, *122*(7–8), 963–978. <https://doi.org/10.1130/B30287.1>
- Gomberg, J., & Davis, S. (1996). Stress/strain changes and triggered seismicity at the Geysers, California. *Journal of Geophysical Research*, *101*(B1), 733–749. <https://doi.org/10.1029/95JB03250>

- Gu, J.-C., Rice, J. R., Ruina, A. L., & Tse, S. T. (1984). Slip motion and stability of a single degree of freedom elastic system with rate and state dependent friction. *Journal of the Mechanics and Physics of Solids*, 32(3), 167–196. [https://doi.org/10.1016/0022-5096\(84\)90007-3](https://doi.org/10.1016/0022-5096(84)90007-3)
- Gu, Y., & Wong, T.-F. (1994). Nonlinear dynamics of the transition from stable sliding to cyclic stick-slip in rock. In *Nonlinear dynamics and predictability of geophysical phenomena* (pp. 15–35). American Geophysical Union (AGU). <https://doi.org/10.1029/GM083p0015>
- Gulia, L., & Wiemer, S. (2019). Real-time discrimination of earthquake foreshocks and aftershocks. *Nature*, 574(7777), 193–199. <https://doi.org/10.1038/s41586-019-1606-4>
- Hawthorne, J. C., & Rubin, A. M. (2010). Tidal modulation of slow slip in Cascadia. *Journal of Geophysical Research*, 115(B9), 668. <https://doi.org/10.1029/2010JB007502>
- Heslot, F., Baumberger, T., Perrin, B., Caroli, B., & Caroli, C. (1994). Creep, stick-slip, and dry-friction dynamics: Experiments and a heuristic model. *Physical Review E*, 49(6), 4973–4988. <https://doi.org/10.1103/PhysRevE.49.4973>
- Hill, D. P., Reasenber, P. A., Michael, A., Arabaz, W. J., Beroza, G., Brumbaugh, D., et al. (1993). Seismicity remotely triggered by the magnitude 7.3 Landers, California, earthquake. *Science*, 260(5114), 1617–1623. <https://doi.org/10.1126/science.260.5114.1617>
- Hong, T., & Marone, C. (2005). Effects of normal stress perturbations on the frictional properties of simulated faults. *Geochemistry, Geophysics, Geosystems*, 6(3), Q03012. <https://doi.org/10.1029/2004GC000821>
- Ide, S. (2010). Striations, duration, migration and tidal response in deep tremor. *Nature*, 466(7304), 356–359. <https://doi.org/10.1038/nature09251>
- Ikari, M. J., Niemeijer, A. R., & Marone, C. (2015). Experimental investigation of incipient shear failure in foliated rock. *Journal of Structural Geology*, 77, 82–91. <https://doi.org/10.1016/j.jsg.2015.05.012>
- Johnson, P. A., Savage, H., Knuth, M., Gombert, J., & Marone, C. (2008). Effects of acoustic waves on stick-slip in granular media and implications for earthquakes. *Nature*, 451(7174), 57–60. <https://doi.org/10.1038/nature06440>
- Kato, A., Obara, K., Igarashi, T., Tsuruoka, H., Nakagawa, S., & Hirata, N. (2012). Propagation of slow slip leading up to the 2011 M w 9.0 Tohoku-Oki earthquake. *Science*, 335(6069), 705–708. <https://doi.org/10.1126/science.1215141>
- Kilgore, B., Beeler, N. M., Lozos, J., & Oglesby, D. (2017). Rock friction under variable normal stress. *Journal of Geophysical Research: Solid Earth*, 122(9), 7042–7075. <https://doi.org/10.1002/2017JB014049>
- Kilgore, B., Lozos, J., Beeler, N., & Oglesby, D. (2012). Laboratory observations of fault strength in response to changes in normal stress. <https://doi.org/10.1115/1.4005883>
- Lambert, A., Kao, H., Rogers, G., & Courtier, N. (2009). Correlation of tremor activity with tidal stress in the northern Cascadia subduction zone. *Journal of Geophysical Research*, 114(B8), B00A08. <https://doi.org/10.1029/2008JB006038>
- Leeman, J. R., Marone, C., & Saffer, D. M. (2018). Frictional mechanics of slow earthquakes. *Journal of Geophysical Research: Solid Earth*, 123(9), 7931–7949. <https://doi.org/10.1029/2018JB015768>
- Leeman, J. R., Saffer, D. M., Scuderi, M. M., & Marone, C. (2016). Laboratory observations of slow earthquakes and the spectrum of tectonic fault slip modes. *Nature Communications*, 7(1), 11104. <https://doi.org/10.1038/ncomms11104>
- Lei, X., & Ma, S. (2014). Laboratory acoustic emission study for earthquake generation process. *Earthquake Science*, 27(6), 627–646. <https://doi.org/10.1007/s11589-014-0103-y>
- Linker, M. F., & Dieterich, J. H. (1992). Effects of variable normal stress on rock friction: Observations and constitutive equations. *Journal of Geophysical Research*, 97(B4), 4923–4940. <https://doi.org/10.1029/92JB00017>
- Lockner, D. A., & Beeler, N. M. (1999). Premonitory slip and tidal triggering of earthquakes. *Journal of Geophysical Research*, 104(B9), 20133–20151. <https://doi.org/10.1029/1999JB900205>
- Logan, J. M., Friedman, M., Higgs, N., Dengo, C., & Shimamoto, T. (1979). Experimental studies of simulated fault gouge and their application to studies of natural fault zones. In *Proceedings of conference VIII—Analysis of actual fault zones in Bedrock, US Geological Survey Open file report* (Vol. 79-1239, pp. 101–120).
- Lowry, A. R. (2006). Resonant slow fault slip in subduction zones forced by climatic load stress. *Nature*, 442(7104), 802–805. <https://doi.org/10.1038/nature05055>
- Marone, C. (1998). Laboratory-derived friction laws and their application to seismic faulting. *Annual Review of Earth and Planetary Sciences*, 26(1), 643–696. <https://doi.org/10.1146/annurev.earth.26.1.643>
- Marone, C., Cocco, M., Richardson, E., & Tinti, E. (2009). The critical slip distance for seismic and aseismic fault zones of finite width. *International Geophysics*, 94, 135–162. [https://doi.org/10.1016/S0074-6142\(08\)00006-5](https://doi.org/10.1016/S0074-6142(08)00006-5)
- Marone, C., & Kilgore, B. (1993). Scaling of the critical slip distance for seismic faulting with shear strain in fault zones. *Nature*, 362(6421), 618–621. <https://doi.org/10.1038/362618a0>
- Mele Veedu, D., Giorgetti, C., Scuderi, M., Barbot, S., Marone, C., & Colletini, C. (2020). Bifurcations at the stability transition of earthquake faulting. *Geophysical Research Letters*, 47(19), e2020GL087985. <https://doi.org/10.1029/2020GL087985>
- Miyazawa, M., & Brodsky, E. E. (2008). Deep low-frequency tremor that correlates with passing surface waves. *Journal of Geophysical Research*, 113(B1). <https://doi.org/10.1029/2006JB004890>
- Miyazawa, M., & Mori, J. (2005). Detection of triggered deep low-frequency events from the 2003 Tokachi-oki earthquake. *Geophysical Research Letters*, 32, 10. <https://doi.org/10.1029/2005GL022539>
- Miyazawa, M., & Mori, J. (2006). Evidence suggesting fluid flow beneath Japan due to periodic seismic triggering from the 2004 Sumatra-Andaman earthquake. *Geophysical Research Letters*, 33(5), L04309. <https://doi.org/10.1029/2005GL025087>
- Nakata, R., Suda, N., & Tsuruoka, H. (2008). Non-volcanic tremor resulting from the combined effect of Earth tides and slow slip events. *Nature Geoscience*, 1(10), 676–678. <https://doi.org/10.1038/ngeo288>
- Noël, C., Giorgetti, C., Scuderi, M. M., Colletini, C., & Marone, C. (2023). The effect of shear displacement and wear on fault stability: Laboratory constraints. *Journal of Geophysical Research: Solid Earth*, 128(4), e2022JB026191. <https://doi.org/10.1029/2022JB026191>
- Noël, C., Passelègue, F. X., Giorgetti, C., & Violay, M. (2019). Fault reactivation during fluid pressure oscillations: Transition from stable to unstable slip. *Journal of Geophysical Research: Solid Earth*, 124(11), 10940–10953. <https://doi.org/10.1029/2019JB018517>
- Noël, C., Pimienta, L., & Violay, M. (2019). Time-dependent deformations of Sandstone during pore fluid pressure oscillations: Implications for natural and induced seismicity. *Journal of Geophysical Research: Solid Earth*, 124(1), 801–821. <https://doi.org/10.1029/2018JB016546>
- Obara, K., & Kato, A. (2016). Connecting slow earthquakes to huge earthquakes. *Science*, 353(6296), 253–257. <https://doi.org/10.1126/science.aaf1512>
- Peng, Z., & Chao, K. (2008). Non-volcanic tremor beneath the central range in Taiwan triggered by the 2001 Mw 7.8 Kunlun earthquake. *Geophysical Journal International*, 175(2), 825–829. <https://doi.org/10.1111/j.1365-246X.2008.03886.x>
- Peng, Z., Vidale, J. E., Wech, A. G., Nadeau, R. M., & Creager, K. C. (2009). Remote triggering of tremor along the san Andreas fault in central California. *Journal of Geophysical Research*, 114(B7), 195. <https://doi.org/10.1029/2008JB006049>
- Perfettini, H., Schmittbuhl, J., Rice, J. R., & Cocco, M. (2001). Frictional response induced by time-dependent fluctuations of the normal loading. *Journal of Geophysical Research*, 106(B7), 13455–13472. <https://doi.org/10.1029/2000JB900366>

- Pignatelli, F., Giorgetti, C., Noèl, C., Marone, C., Collettini, C., & Scuderi, M. M. (2023). The effect of normal stress oscillations on fault slip behavior near the stability transition from stable to unstable motion [Dataset]. Zenodo. <https://doi.org/10.5281/zenodo.8131061>
- Pollitz, F. F., Stein, R. S., Sevilgen, V., & Bürgmann, R. (2012). The 11 April 2012 east Indian Ocean earthquake triggered large aftershocks worldwide. *Nature*, *490*(7419), 250–253. <https://doi.org/10.1038/nature11504>
- Rathbun, A. P., & Marone, C. (2010). Effect of strain localization on frictional behavior of sheared granular materials. *Journal of Geophysical Research*, *115*(B1), 615. <https://doi.org/10.1029/2009JB006466>
- Rice, J. R. (1993). Spatio-temporal complexity of slip on a fault. *Journal of Geophysical Research*, *98*(B6), 9885–9907. <https://doi.org/10.1029/93JB00191>
- Rice, J. R., & Ruina, A. L. (1983). Stability of steady frictional slipping. *Journal of Applied Mechanics*, *50*(2), 343–349. <https://doi.org/10.1115/1.3167042>
- Richardson, E., & Marone, C. (1999). Effects of normal stress vibrations on frictional healing. *Journal of Geophysical Research*, *104*(B12), 28859–28878. <https://doi.org/10.1029/1999JB900320>
- Rubinstein, J. L., La Rocca, M., Vidale, J. E., Creager, K. C., & Wech, A. G. (2008). Tidal modulation of nonvolcanic tremor. *Science*, *319*(5860), 186–189. <https://doi.org/10.1126/science.1150558>
- Rubinstein, J. L., Vidale, J. E., Gombert, J., Bodin, P., Creager, K. C., & Malone, S. D. (2007). Non-volcanic tremor driven by large transient shear stresses. *Nature*, *448*(7153), 579–582. <https://doi.org/10.1038/nature06017>
- Ruina, A. (1983). Slip instability and state variable friction laws. *Journal of Geophysical Research*, *88*(B12), 10359–10370. <https://doi.org/10.1029/JB088iB12p10359>
- Rydelek, P. A., Sacks, I. S., & Scarpa, R. (1992). On tidal triggering of earthquakes at Campi Flegrei, Italy. *Geophysical Journal International*, *109*(1), 125–135. <https://doi.org/10.1111/j.1365-246X.1992.tb00083.x>
- Savage, H. M., & Marone, C. (2007). Effects of shear velocity oscillations on stick-slip behavior in laboratory experiments. *Journal of Geophysical Research*, *112*(B2), B02301. <https://doi.org/10.1029/2005JB004238>
- Savage, H. M., & Marone, C. (2008). Potential for earthquake triggering from transient deformations. *Journal of Geophysical Research*, *113*(B5), B05302. <https://doi.org/10.1029/2007JB005277>
- Scholz, C. H. (2003). Good tidings. *Nature*, *425*(6959), 670–671. <https://doi.org/10.1038/425670a>
- Scholz, C. H., Tan, Y. J., & Albino, F. (2019). The mechanism of tidal triggering of earthquakes at mid-ocean ridges. *Nature Communications*, *10*(1), 2526. <https://doi.org/10.1038/s41467-019-10605-2>
- Scuderi, M. M., Collettini, C., Viti, C., Tinti, E., & Marone, C. (2017). Evolution of shear fabric in granular fault gouge from stable sliding to stick slip and implications for fault slip mode. *Geology*, *45*(8), 731–734. <https://doi.org/10.1130/G39033.1>
- Scuderi, M. M., Marone, C., Tinti, E., Di Stefano, G., & Collettini, C. (2016). Precursory changes in seismic velocity for the spectrum of earthquake failure modes. *Nature Geoscience*, *9*(9), 695–700. <https://doi.org/10.1038/ngeo2775>
- Shelly, D. R., Beroza, G. C., & Satoshi, I. (2007). Complex evolution of transient slip derived from precise tremor locations in western Shikoku, Japan. *Geochemistry, Geophysics, Geosystems*, *8*(10), Q10014. <https://doi.org/10.1029/2007GC001640>
- Shelly, D. R., Peng, Z., Hill, D. P., & Aiken, C. (2011). Triggered creep as a possible mechanism for delayed dynamic triggering of tremor and earthquakes. *Nature Geoscience*, *4*(6), 384–388. <https://doi.org/10.1038/ngeo1141>
- Shreedharan, S., Bolton, D. C., Rivière, J., & Marone, C. (2020). Preseismic fault creep and elastic wave amplitude precursors scale with lab earthquake magnitude for the continuum of tectonic failure modes. *Geophysical Research Letters*, *47*(8), e2020GL086986. <https://doi.org/10.1029/2020GL086986>
- Shreedharan, S., Rivière, J., Bhattacharya, P., & Marone, C. (2019). Frictional state evolution during normal stress perturbations probed with ultrasonic waves. *Journal of Geophysical Research: Solid Earth*, *124*(6), 5469–5491. <https://doi.org/10.1029/2018JB016885>
- Stein, R. S., King, G. C., & Lin, J. (1992). Change in failure stress on the southern San Andreas fault system caused by the 1992 magnitude = 7.4 Landers earthquake. *Science*, *258*(5086), 1328–1332. <https://doi.org/10.1126/science.258.5086.1328>
- Thomas, A. M., Nadeau, R. M., & Bürgmann, R. (2009). Tremor-tide correlations and near-lithostatic pore pressure on the deep San Andreas fault. *Nature*, *462*(7276), 1048–1051. <https://doi.org/10.1038/nature08654>
- Townend, J., & Zoback, M. D. (2000). How faulting keeps the crust strong. *Geology*, *28*(5), 399–402. [https://doi.org/10.1130/0091-7613\(2000\)28<399:hftcs>2.0.co;2](https://doi.org/10.1130/0091-7613(2000)28<399:hftcs>2.0.co;2)
- Tullis, T. E., & Weeks, J. D. (1986). Constitutive behavior and stability of frictional sliding of granite. *Pure and Applied Geophysics*, *124*(3), 383–414. <https://doi.org/10.1007/BF00877209>
- van der Elst, N. J., Nicholas, J., Keranen, K. M., & Abers, G. A. (2013). Enhanced remote earthquake triggering at fluid-injection sites in the midwestern United States. *Science*, *341*(6142), 164–167. <https://doi.org/10.1126/science.1238948>
- Vidale, J. E., Agnew, D. C., Johnston, M. J. S., & Oppenheimer, D. H. (1998). Absence of earthquake correlation with Earth tides: An indication of high preseismic fault stress rate. *Journal of Geophysical Research*, *103*(B10), 24567–24572. <https://doi.org/10.1029/98JB00594>